Environmental Forcing of Super Typhoon Paka's (1997) Latent Heat Structure

Edward Rodgers[1], William Olson[2], Jeff Halverson[2], Joanne Simpson[1], and Harold Pierce[3]

1 Laboratory for Atmosphere NASA/Goddard Space Flight Center, Greenbelt MD, 20771.

2 JCET/University of Maryland, Baltimore County, Code 912, NASA/Goddard Space Flight Center, Greenbelt MD, 20771

3 Science and System Application Inc., Lanham, MD, 20706

October 1999

Submitted to Journal of Applied Meteorology

Corresponding author address: Dr. Edward B. Rodgers Mesoscale Atmospheric Processing Branch (Code 912), Laboratory for Atmosphere NASA/Goddard Space Flight Center, Greenbelt MD, 20771. Email address: rodgers@agnes.gsfc.nasa.gov

ABSTRACT

The distribution and intensity of total (i.e., combined stratified and convective processes) rainrate/latent heat release (LHR) were derived for tropical cyclone Paka during the period 9-21 December, 1997 from the F-10, F-11, F-13, and F-14 Defense Meteorological Satellite Special Sensor Microwave/Imager and the Tropical Rain Measurement Mission Microwave Imager observations. These observations were frequent enough to capture three episodes of inner core convective bursts that preceded periods of rapid intensification and a convective rainband (CRB) cycle. During these periods of convective bursts, satellite sensors revealed that the rainrates/LHR: 1) increased within the inner eye wall region; 2) were mainly convectively generated (nearly a 65% contribution), 3) propagated inwards; 4) extended upwards within the middle and upper-troposphere, and 5) became electrically charged. These factors may have caused the eye wall region to become more buoyant within the middle and upper-troposphere, creating greater cyclonic angular momentum, and, thereby, warming the center and intensifying the system.

Radiosonde measurements from Kwajalein Atoll and Guam, sea surface temperature observations, and the European Center for Medium Range Forecast analyses were used to examine the necessary and sufficient condition for initiating and maintaining these inner core convective bursts. For example, the necessary conditions such as the atmospheric thermodynamics (i.e., cold tropopause temperatures, moist troposphere, and warm SSTs [>26°]) suggested that the atmosphere was ideal for Paka's maximum potential intensity (MPI) to approach super-typhoon strength. Further, Paka encountered weak vertical wind shear (<15 ms^{-1}) before interacting with the westerlies on 21 December. The sufficient conditions, on the other hand, appeared to have some influence on Paka's convective burst, but the horizontal moisture flux convergence values in the outer core were weaker than some of the previously examined tropical cyclones. Also, the upper tropospheric outflow generation of eddy relative angular momentum flux convergence was much less than that found during moderate tropical cyclone/trough interaction. These results indicated how important the external necessary condition and the internal forcing (i.e., CRB cycle) were in generating Paka's convective bursts as compared to the external sufficient forcing mechanisms found in higher latitude tropical cyclones. Later, as Paka began to interact with the westerlies, both the necessary (i.e., strong vertical shear and colder SSTs) and sufficient (i.e., dry air intrusion) external forcing mechanisms helped to decrease Paka's rainrate.

1. Introduction

Tropical cyclone case studies of Hurricane Opal (Rodgers et al. 1998); Typhoon Bobbie (Rodgers and Pierce 1995); and Hurricanes Dean, Gabrielle, and Hugo (Rodgers et al. 1994) that used both the F-10, F-11, F-13, and the F-14 Defense Meteorological Satellite Program (DMSP) Special Sensor Microwave/Imager (SSM/I's) observations to estimate cloud microphysics and the European Center for Medium-Range Weather Forecasting (ECMWF) analyses to derive tropical cyclone environmental forcing mechanisms suggested the following. First, the convective rainband (CRB) cycles (Willoughby 1988; 1990 and Willoughby et al. 1982), warm SSTs, and large scale environmental forcing had a profound effect on the evolution of the release of latent heat in the middle and upper troposphere of their inner core region (i.e., within the 111 km radius [Weatherford 1987]) and subsequent hurricane intensity. Second, the CRB cycles appeared to be initiated by lower-tropospheric horizontal moisture flux convergence over oceanic regions where SSTs were warmer than 26° C, the tropospheric conditions were uniformly moist, and the vertical wind shear was less than 10 m s^{-1}. Finally, the increase of eyewall/inner core latent heat appeared to be enhanced by the inward propagation of the CRBs and/or by the gradient wind adjustment processes associated with the thermally direct circulation in the entrance regions of the upper-tropospheric outflow channel (Challa and Pfeffer 1980; Merrill 1988; Chen and Gray 1985; Molinari and Vollaro 1989, Shi et al 1990; Rodgers et al. 1991; DeMaria et al. 1993).

However, the Opal analyses (Rodgers et al. 1998) was the only case study for which there were a sufficient number of SSM/I observations to resolve the large scale rainrate oscillations. Furthermore, the majority of the previous studies did not incorporate other remotely sensed data that helped validate the hypotheses concerning cloud microphysics and sparse upper-tropospheric circulation observations.

This case study differs from previous ones by employing the following additional satellite borne sensors. First, the monitoring of the evolution of Paka's spatial distribution of rainrate and latent heat release (LHR) profiles by SSM/Is will be improved by adding the Tropical Rainfall Measuring Mission's (TRMM's) Microwave Imager (TMI) observations. Second, lightning data obtained from the Optical Transient Detector (OTD) sensor and the TRMM's Lightning Imaging Sensor (LIS) will help assess the electrically active convective regions of Paka. Finally, the Earth Probe total ozone mapping spectrometer (TOMS) and the Geosynchronous Meteorological Satellite (GMS)-derived upper-tropospheric water vapor and water vapor winds will help substantiate the ECMWF analyses of the upper-tropospheric circulation.

In this paper, Section 2 describes the satellites and their sensors, the satellite observed parameters, and how these parameters are obtained. Section 3 includes a description of the environmental forcing parameters obtained from the Goddard Data Assimilation Office (DAO) and the ECMWF analyses. A brief narration of the time history of tropical cyclone Paka is presented in Section 4, while Section 5 details the evolution of the distribution of Paka's total rainrate/LHR and its relationship to intensity change. Section 6 identifies possible environmental parameters that favor Paka's rainrate/latent heat growth and its subsequent intensification. Finally, a summary and discussion of the Paka case study is presented in section 7.

2. Satellite-observed Parameters

TABLE 1

SATELLITE	SOURCE	PARAMETER
GMS*	Cloud top temperature	Maximum sustained surface winds, cloud height, buoyancy, & eye size
	Water vapor channel	Upper-tropospheric water vapor & winds
EARTH PROBE	TOMS*	Total ozone, potential vorticity fields, & tropopause topography
DMSP*	SSM/I*	Rainrates, total LHR, latent heat profiles, & precipitable water
OTD*	OTD	Lightning
TRMM*	TMI*	Rainrates, total LHR, & latent heating profiles
	LIS*	Lightning

*

GMS - Geosynchronous Meteorological Satellite

TOMS - Total Ozone Mapping Spectrometer

DMSP - Defense Meteorological Satellite Program

SSM/I - Special Sensor Microwave/Imager

OTD - Optical Transient Detector

TRMM - Tropical Rainfall Measuring Mission

TMI - TRMM Microwave Imager

LIS - Lightning Imaging Sensor

Table 1 lists the satellites, the sensors, and the satellite-derived parameters that are utilized in this study. The SSM/I is employed to estimate rainrate, LHR, and total

precipitable water (TPW), while the TMI is used to only estimate rainrate and LHR. The OTD and LIS monitors Paka's electric activity. These satellite observations also help to qualitatively assess the buoyancy of the convective regions of Paka. The SSM/I derived TPW is employed to justify the ECMWF-derived moisture distribution. The rapid observations from the GMS-observed infrared (11.5 um window channel) blackbody temperatures (T_{BB}) are utilized to estimate Paka's lower and upper-tropospheric winds, intensity (using the Dvorak technique [Dvorak 1974]), eye size, and to qualitatively verify whether SSM/I and TMI observation are capturing the major temporal changes of Paka's mean rainrate. Finally, the GMS-observed upper-tropospheric water vapor and derived water vapor winds as well as the Earth Probe TOMS-estimated total ozone help to qualitatively verify the ECMWF-derived upper-tropospheric environmental circulation. Further information concerning the OTD, LIS, TOMS, and GMS sensors and their derived parameters can be found in Appendix A.

a Special Sensor Microwave/Imager (SSM/I)-estimated rainrate and LHR parameters

1) THE F-11, F-13, AND F-14 DMSP SSM/Is

The SSM/Is on board DMSP F-11, F-13, and F-14 satellites that were launched, respectively, in November, 1992, May 1995, and April 1997 measure scattered and emitted microwave radiation at frequencies of 19.35, 22.25, 37.0, and 85.5 GHz. All channels except the 22.25 GHz channel are dual polarized. The SSM/Is complete 14.1 revolutions per day along a nearly sun-synchronous polar orbit at an altitude of 833 km. The approximate times that the ascending branches of the DMSP F-11, F-13, and F-14 orbits pass over the Equator at 165° E (i.e., the approximate central location of tropical cyclone Paka during 9-22 December, 1997) are, respectively, 0800, 0700, 0900 UTC, while the descending branches occur 12 hours later. The SSM/Is scan conically at a constant 45°

angle from nadir and have an observational swath width of nearly 1400 km at the earth's surface. Further information concerning the SSM/I sensor and measurements may be found in Hollinger (1991).

2) SSM/I-ESTIMATED RAINRATES, CONVECTIVE RAIN FRACTION, AND LATENT HEATING PROFILES

The surface rainrate, convective rain fraction, and latent heating profiles are retrieved from all the SSM/I channels by employing the Goddard Profiling Algorithm (GPROF). This algorithm uses the estimated expected value, or "Bayesian" method described by Kummerow et al. (1996), Olson et al. (1996), and Olson et al. (1999). All three parameters are retrieved at a horizontal resolution of 12.5 km X 12.5 km. The surface rainrates are defined as the average rainrate over the 12.5 km X 12.5 km area centered on the SSM/I observation.

The convective rain fraction is the fraction of the surface rainrate associated with significant cloud updrafts and downdrafts ($| w |_{> 1\ m\ s^{-1}}$). The LHR at a given level is the net energy release per unit volume of air due to hydrometer phase changes (i.e., condensation/evaporation, deposition/sublimation, and freezing/melting), averaged over the same 12.5 km X 12.5 km area. Further description of the retrieval method and supporting numerical atmospheric model simulations are found in the appendix of Rodgers et al. (1998) and Olson et el. (1999).

3) SSM/I-ESTIMATED TOTAL PRECIPITABLE WATER (TPW)

The SSM/I-estimated TPW over ocean regions is derived from an algorithm developed by Petty and Katsaros (1990). The algorithm is based upon a logarithmic

regression equation relating rawindsonde-observed TPW to the SSM/Is dual polarized 19.35 GHz and vertically polarized 23.25 GHz channel. The SSM/I algorithm cannot retrieve TPW over land and in raining ocean areas.

b . TRMM Microwave Imager (TMI)-estimated rainrate and LHR parameters

1) THE TRMM TMI

The TRMM-based TMI was launched in November 1997 and measures scattered and emitted microwave radiation at frequencies at 10.7, 19.4, 21.3, 37.0, and 85.5 GHz. All channels, except the 21.3 GHz channel, are dual polarized. The TRMM satellite has a circular orbit with an altitude of 350 km, an inclination of 35° to the Equator, and observes a swath width of 790 km at the earth's surface. Diffraction effects and the fixed antenna size of the TMI cause the instantaneous field of view (IFOV) to increase with decreasing channel frequency. For example, the 85.5 GHz channel IFOV is 4.4 km, while IFOV of the 10.7 GHz channel is 40 km. The satellite completes 16 orbits per day and the TRMM orbit processes such that Paka's overpass times vary during the study period. Further information concerning the TMI sensor and measurements may be found in Simpson et al. (1995), Simpson et al. (1988), and Kummerow et al. (1998).

2) TMI-ESTIMATED RAINRATES, CONVECTIVE RAIN FRACTION, AND LATENT HEATING PROFILES

The TMI-derived surface rainrate, convective rain fraction, and latent heating rate profile are retrieved using the same SSM/I algorithm (i.e., GPROF). However, the surface rainrates are averaged over a 10.0 km X 10.0 km area centered on the TMI observation. Other TMI observational differences are the improved IFOV and the employment of 10.7

GHz channel in its algorithm. Further description of the SSM/I retrieval method and supporting numerical atmospheric model simulations are found in the appendix of Rodgers et al. (1998) and from Olson et el. (1999).

3. Model-derived and archived environmental and tropical cyclone parameters

TABLE 2

SOURCE	ANALYSES	PARAMETER
DAO* ARCHIVES	SSTs*	Oceanic energy flux
ECMWF* MODEL	150 hPa geopotential heights	Upper-tropospheric topography
	150 hPa horizontal divergence	Upper-tropospheric divergence
	200 - 850 hPa vertical shear	Tropospheric wind shear
	Total precipitable water	Tropospheric precipitable water distribution
	400-1000 hPa HMF*	Tropospheric water vapor flux
	Vertical distributed equivalent potential temperature	Tropospheric moisture
	200 hPa ERFC*	Tropical cyclone azimuthally mean ERFC
	100-200 hPa PV*	Upper-tropospheric potential vorticity fields
	850 hPa HMF*	Lower-tropospheric water vapor flux

*

DAO - Data Assimilation Office

SSTs - Sea Surface Temperatures

ECMWF - European Center of Medium-Range Weather Forecasting

ERFC - Eddy Relative Angular Momentum Flux Convergence

PV - Potential Vorticity

HMF - Horizontal Moisture Flux

Tables 2 list the parameters that are estimated and derived, respectively, from the Goddard Center Analyses Office (DAO) archives and the ECMWF analyses. A brief description of these parameters is as follows.

a Sea Surface Temperature

To determine whether the SSTs are warm enough (i.e., SST>26°) to allow for sufficient moist static energy flux to support convection in tropical cyclone Paka, mean weekly SSTs within the regions that Paka traversed are examined. The weekly mean SSTs on a 1.0° latitude X 1.0° longitude grid are obtained from National Center for Environmental Prediction (NCEP) analyses that are archived at Goddard's DAO. The SSTs that Paka traversed are estimated for a given location by interpolating the SSTs near the center of Paka at a twelve-hour interval from the given weekly SSTs. To eliminate discontinuities in the SSTs between the weeks, the SSTs at each 12-hour interval are time weighted between the weekly means.

b ECMWF-Derived Environmental Parameters

The upper- and lower-tropospheric external environmental forcing mechanisms in regions of weak inertial stability are also examined for their role in initiating, maintaining, and inhibiting Paka's total rainrate/LHR cycle. The forcing mechanisms analyzed in this study are the vertical wind shear, the lower-tropospheric horizontal moisture flux, and the upper-tropospheric gradient wind adjustment processes associated with Paka's outflow jet-induced ERFC. These external forcing parameters are similar to those used in NOAA's Statistical Hurricane Intensity Prediction Scheme (SHIPS) (DeMaria and Kaplan (1994), except for the horizontal tropospheric moisture flux.

The upper and lower-tropospheric parameters are obtained from the European Center for Medium-Range Weather Forecasts (ECMWF) (Shaw et al. 1987) diagnostic program. The ECMWF analyses are archived on a 2.5° latitude X 2.5° longitude grids and the environmental parameters are calculated every 12 hours (i.e., at 0000 UTC and 1200 UTC) by using the GEMPAK 5.1 (des Jardins et al. 1991).

The preference of ECMWF analyses is based on the fact that the wind, height, and moisture fields are less noisy in data-void North Pacific regions and that the model employs NOAA, GMS, and TIROS-N TOVS-observed temperature, thickness, and wind data in their analyses. It has also been shown that the model generates more accurate analyses of tropical systems over data void eastern North Atlantic Ocean regions (Reed et al. 1988). However, because of the poor spatial resolution of the ECMWF analyses and the lack of observations, finer scale features surrounding Paka's central dense overcast (CDO) are not always captured. Nevertheless, the ECMWF analyses of the upper-tropospheric wind and lower-tropospheric TPW within Paka's environment may be improved by using, respectively, the GMS-derived water vapor winds and SSM/I-derived TPW. The ECMWF grid analyses at finer time and space resolution were not readily available for this study. A

more detailed description of the parameters that are employed in this study can be found in Appendix B.

4 Tropical Cyclone Paka

A region of organized convection that was associated with an equatorial westerly wind burst was first observed late November during the strong El Niño of 1997 approximately 2000 km southwest of the Hawaiian Islands. The dual cyclonic vorticity regions associated with the westerly wind burst led to the formation of twin tropical cyclones, one in the Southern Hemisphere named Pam and the other in the Northern Hemisphere named Paka. During the first week in December, tropical cyclone Paka, the system of concern, reached tropical storm stage as it moved rapidly west northwestward over the open North Central Pacific at relatively low latitudes. The system reached typhoon stage on 10 December, super-typhoon stages on 15 and again on 18 December, and then quickly dissipated on 21 December. Typhoon Paka's west-northwest movement across the central and western North Pacific during 9-21 December brought the system just south of the Majuro and Kwajalein Atolls between 10 and 12 December and just north of Guam on 16 December. A plan view of Paka's location and intensity status during this time are seen in Fig. 1. Information concerning the intensity and position of tropical cyclone Paka can be found at the National Climate Data Center.

5 Time history of Paka's rainrate, latent heating, and lightning distribution

a Inner core total rainrate versus intensity

To estimate the evolution of Paka's inner core mean total rainrate, the SSM/I and TMI-derived rainrates are azimuthally averaged over the inner core area. Fig. 2 shows a time series of Paka's maximum surface wind speeds every 6 hours and the SSM/I (open circles) and TMI (X) derived inner-core averaged rainrates. Between 9-21 December there were 19 SSM/I and 9 TMI observations, with at least one rainrate observation during each day, except on 20 December.

It is seen in Fig. 2 that there are three episodes when the long-term trend in the inner-core mean-total rainrates increase significantly. These episodes occur approximately 10-12, 13-14, and 16-17 December. During the first episode, rainrates increased by more than 3 mm h^{-1}, while during the second and third episodes they increased, respectively, by approximately 2 and 4 mm h^{-1}. These three periods appear to precede the times of maximum surface winds. The figure also suggests that as Paka became more intense, the response time between enhanced rainrates and increased surface winds decreased. This increased response time has been suggested by Baik (1993) to be related to the increase of the middle- and lower-tropospheric inner core inertial stability, which is a function of tangential winds and coriolis force.

By comparing the evolution of Paka's eye with the inner core rainrates that have been interpolated (using a spline fit) over a 6 hour interval (Fig. 3), it is observed that the eye was present during and preceding large increases of inner core rainrates. The figure shows that the GMS, SSM/I, and TMI detected an eye on 11, 14-15, and 17-18 December. The radius of the eye became progressively larger (5 km to 20 km) as Paka evolved. It is also seen that during the later stages of development (17-18 December) when Paka's maximum winds peaked, the eye radius reached its maximum radius. This suggests that when the eye became more visible within the CDO, the buoyancy of the eye wall reached its maximum, the horizontal convergence and subsidence in the upper-tropospheric region

of the eye increased, the eye warmed, and the tropical cyclone approached maximum intensity.

However, it is not obvious that the SSM/I and TMI observations are frequent enough to accurately delineate the large-scale oscillations in Paka's inner core averaged rainrates. If it is assumed that increased ascending motion in the inner core regions corresponds to colder mean CDO T_{BB} and greater rainrates, it may be possible to qualitatively verify the large scale relative change of Paka's SSM/I and TMI-derived rainrates with the more frequently observed GMS infrared-derived mean inner core CDO T_{BB}.

To qualitatively verify whether the SSM/I and TMI observations are capturing the major temporal changes of Paka's inner core mean rainrate, the 10% smoothed hourly observed GMS infrared (11.0 um) mean T_{BB} averaged over the inner core region is compared to the evolution of the six hour interval SSM/I and TMI-derived mean rainrate (Fig. 4). Considering the fact that: 1) sampling the eye may overestimate the mean CDO T_{BB}; 2) thick cirrus debris left by the initial convection may mask future lower active convective cells and, therefore, cause the minimum mean CDO T_{BB} to precede the time of maximum mean rainrates; and 3) that the convective cells dissipate from the bottom upwards, which causes the minimum mean CDO T_{BB} to follow the time of maximum inner core rainrate, there is reasonable consistency between these parameters. Except for the third episode of increasing rainrates on 17 December when the sampling of the large eye caused an over-estimation of the CDO T_{BB}, the trend in the GMS mean inner core CDO T_{BB} appears to capture the major changes in Paka's inner core mean rainrate. This mean inner core CDO T_{BB} curve in Fig. 4 suggests that there are frequent enough SSM/I and TMI observations to define the majority of the large time scale temporal changes in Paka's inner core rainrate cycle.

b Percent of convectively generated LHR in Paka's inner core

It is seen in Fig. 5 that the trend of the rainrate generated by convective processes, although less approximately mirrors the trend of total rainrate. The greatest percent of contribution was approximately 65%, which occurs during episodes of maximum total rainrate. These values were slightly less than that found with tropical cyclone Opal's episodes of maximum total latent heat release (Rodgers et al. 1998), but consistent with those derived from airborne radar in earlier hurricane case studies (Marks 1985; Marks and Houze 1987). Since the greatest contribution of total rainrate was from convective processes during episodes of maximum total rainrates, these episodes will be referred to as convective bursts in the remainder of the text.

c Radial-time distribution of Paka's convective rainrate

To examine the temporal change of Paka's horizontal distribution of convective rainrates during the period of 8-21 December 1997, all available SSM/I and TMI-derived convective rainrates of Paka are azimuthally averaged over sixteen annuli, each 27.5 km in width, extending outward from Paka's center to 444 km radius. The averaged convective rainrate values in each annuli are, again, interpolated to 6 hour intervals using a spline fit and are presented in a time-radius format in Fig. 6. Also plotted with these azimuthally averaged rainrates are Paka's 6-hour interval maximum surface winds.

Although the convective rainrates are averaged over large annular areas, the evolution of the three periods of convective bursts is clearly delineated. Similar to what was seen in Fig. 2, Fig. 6 indicates that the periods of increasing inner core rainrate precede the time of maximum surface winds. This inner core rainrate cycle and intensity

relationship were also revealed in SSM/I observational studies of four 1989 western North Atlantic hurricanes, (Rodgers et al., 1994), western North Pacific Typhoon Bobbie (1992) (Rodgers and Pierce 1995), and the Gulf of Mexico Hurricane Opal (1995) (Rodgers et al. 1998).

The figure also illustrates that prior to the first and third convective bursts, a region of elevated rainrates propagate inwards with time on 11 and 16 December. The inward propagating rain band observed on 16 December appears to delineate the beginning of a CRB cycle. The figure indicates that an outer convective rain band located approximately 111-165 km from Paka's center forms, intensifies, propagates inward, and dissipates the original eye wall (i.e., by either subsidence or by reducing the influx of moisture), thereby initiating a new eye wall (the third convective burst) on 17 December.

d Plan views of Paka's convective rainrate distribution

Clearer evidence of Paka's CRB cycle is presented in Fig. 7. The figure shows six plan views of the distribution of Paka's convective rainrates during the CRB cycle that was derived from SSM/I and TMI observations. The figure illustrates the following series of events. During the period between 0509 UTC on 13 to 0831 UTC on 14 December a crescent shaped eye wall (rainrates > 20 mm h^{-1}) expands and intensifies. Approximately twenty four hours later at 0817 UTC on 15 December, evidence of an outer convective rain band (rainrates > 2 mm h^{-1}) is seen on the outer edge (i.e., ~165 km from the center of circulation) of the convective rain shield. During this time the rainrates in the eye wall appear to decrease in intensity. At 2149 UTC on 15 December, the outer convective rain band grows in area and propagates inwards causing the rainrates in the eye wall to rapidly decrease. At 1425 UTC on 16 December the new eye wall is formed as the outer CRB propagates inwards and generates a well-developed eye wall with an open eye. Finally at

2243 UTC on 16 December (the time of the third convective burst), rainrates in the eye wall rapidly intensify, however, the eye wall becomes more asymmetric and the eye rapidly decreases in size.

The plan views of Paka's convective rain distribution also clearly show the symmetry of its eye wall. It is known that the greater the symmetry of the eye wall, the more concentrated the subsidence-induced warming is at the center, and the more likelihood that the system will intensify.

Examining the plan views of the first convective burst (figure not shown), it is indicated that there is no evidence of a symmetric eye wall prior to the 13 December. However, Fig. 7 clearly shows that early of 17 December as the new eye wall formed during the CRB cycle, it became more symmetric. By 1200 UTC on 17 December the eye wall convective rainrates began to increase more rapidly, but the new eye wall, once again, lost its symmetry as it continued to constrict.

e Vertical distribution of latent heating in Paka's inner core

To estimate the buoyancy of the inner core eye wall (Fitzpatrick 1996) during the CRB cycle, the SSM/I and TMI vertical distributions of the azimuthally averaged total (i.e., combined stratified and convective) latent heating within 333 km radius of Paka's center for the six observation periods described in Fig. 7 are shown in Fig. 8. Evidence of the second convective burst is illustrated by the latent heat profiles seen at 0509 UTC on 13 December and at 0831 UTC on 14 December. These figures suggest that the large net latent heating of 1 W m^{-3} that is observed at 4 km during 0509 UTC on 13 December extends upwards to 10 km at 0831 UTC on 14 December. These maximum latent heating values (greater than 3 W m^{-3}), located in the lower troposphere (< 3 km) at this time were

mainly generated by convective processes (65% as seen in Fig 5) with little loss of latent heat near the surface due to evaporation. On the other hand, in the upper-troposphere above the freezing level, cloud ice microphysical processes generated large amounts of stratiform and convectively induced latent heat on 14 December. These figures also suggested that the deep layer maximum net latent heating is located to within approximately 25 km of the center of circulation. This helped to concentrate and increase the eye wall excess buoyancy nearer to the center and, thereby, enhanced the warming within the eye.

First evidence of an outer convective rainband can be seen at 0817 UTC on 15 December outside the inner core that propagated inwards at 2149 UTC on 15 December. At 0817 on 15 December the eye wall latent heating decreased (i.e., ~2 W m^{-3}) leaving a limited vertical region of maximum latent heat of 1 W m^{-3} near the center at the altitude of 4 km, while the latent heating in the new convective rainband increased to values greater than 1 W m^{-3}. Between 1425 UTC and 2243 UTC on 16 December, the new eye wall that initiated the third convective burst decreased in radius, increased in rainrate, rain volume, and vertical extent. The distribution and net latent heating in the new eye wall appears to be similar too that of the original eye wall.

It is evident from these latent heat profiles that during the CRB cycle the last two convective bursts appear to greatly influence Paka's eye wall buoyancy and its subsequent intensification by generating intense deep layer latent heating near the center of circulation. One theory (Fitzpatrick 1996) suggests that the increased buoyancy created by the excess latent heating helps to compensate for the loss of eye wall cyclonic angular momentum due to surface friction and upper-tropospheric outward transport. The upward transport of cyclonic angular momentum will increase the cyclonic tangential circulation aloft and, thereby, warm the upper-tropospheric eye through thermal wind balance and gradient wind

adjustment processes. The subsidence induced warming in the upper-tropospheric eye, in turn, will hydrostatically lower the surface pressures.

f Lightning distribution

The monitoring of electrical discharge in clouds from satellite can provide substantial information about the distribution of the convective system's LHR, precipitation, cloud microphysics, and buoyancy. This information, in turn, can be used to assess the severity of the weather that the convective system could produce. However, in measuring the electrical discharge in typhoon Paka (as well as most tropical cyclones) from both OTD and LIS there are two major problems that arise.

The first, and most obvious problem, is the infrequent visit time of the OTD and LIS sensors. Because of the different orbital geometries of the satellites and the different IFOVs of the sensors, the approximate number of times each sensor could observe Paka would be at least once a day, and there would be no fixed observational time difference between the sensors.

The second problem is that the vertical motion in the eyewall region (i.e., the region that dictates the intensity of the tropical cyclone) in the majority of the tropical cyclones is less than approximately 10.0 m s^{-1} that is required to generate the cloud microphysical properties necessary for the production of electrical discharges (Molinari et al. 1994; Lyons, W. A. and C. Keen 1994), while vertical velocities in the outer core regions are usually greater. Therefore, using lightning discharge observations to assess the relative buoyancy of the eyewall region of a tropical cyclone may be questionable. However, employing land based sensors that can frequently measure electrical discharge directly in tropical cyclones near the United State coast (National Lightning Detection Network

[Orville et al. 1987]) or indirectly over some of the data void oceans (sferics measurements [Morales et al. 1998]), the inward propagation of convection and/or the CRB cycle can be easily monitored if the outer core convection is highly electrically charged. Unfortunately, Paka was over the western North Pacific, far removed from any ground-based sensors.

Nevertheless, the infrequent observations of lightning discharge in Paka from the LIS and OTD sensors suggest that the greatest number of lightning discharges occurred on 12 (Fig. 9) and 13 December in the southeastern rain bands (greater than 444 km from the center). This result is not surprising, since these outer core rain bands usually have stronger ascending motion than the eyewall regions. However, at approximately 1800 UTC on 12 December, lightning discharges were observed within Paka's inner core (i.e., approximately 50 km north of Paka center [see Fig. 9]) indicating that the inner core was most likely more buoyant (i.e., ascending motion is greater than 10.0 m s^{-1}), producing greater rainrates, and helping Paka to rapidly intensify. It can be seen in Fig. 2 that indeed the inner core lightning discharge occurred prior to the second convective burst on 13 December. After 13 December, the LIS and OTD sensors failed to observe any other lightning discharges in Paka.

6. Time history of the environmental influences on Paka's rainrates and LHR

There are three specific periods of interest during Paka's evolution: 1) the episodes of inner core convective burst that occurred between 10-11 and 13-14 December; 2) the initiation of the CRB cycle that was observed between 15-19 December; and 3) the rapid dissipation of the inner and outer core convection that occurred after 19 December. In order to determine what influence the large-scale external forcing mechanisms had in enhancing, maintaining, and dissipating the inner and outer core convective bursts and

CRB cycle, both the necessary and sufficient forcing conditions are explored. The necessary conditions involve the magnitudes of tropopause temperature, SSTs, and vertical wind shear, that have been shown from many earlier studies to effect a tropical cyclone's intensity, maximum potential intensity (MPI), and its convection are first examined. Then possible sufficient conditions that may have led to the initiation or dissipation of the convective episodes will be examined. Because of the poor spatial and temporal resolution of the ECMWF analyses and the lack of data, no attempt will be made to rigorously connect these sufficient forcing conditions to the distribution and intensity of cloud microphysical properties. Instead, the justification for choosing these forcing conditions will be based on previous research. The forcing conditions will only be involved to suggest processes that may have changed the distribution and intensity of Paka's cloud microphysical properties.

Regarding possible significant environmental forcing conditions, the lower-tropospheric moisture flux convergence is examined first for its role in the initiation and decay of the outer core convective bands. The upper-tropospheric circulation is then examined as it pertains to trough/tropical cyclone interaction, the generation of diffluent outflow channels, and the creation of an inward surge of eddy relative angular momentum.

a Necessary Conditions That May Have Initiated and Maintained The Inner and Outer Core Convective Burst or CRB cycle

1) SEA SURFACE TEMPERATURE

The evolution of SSTs that Paka traversed between 0000 UTC on 9 to 0000 UTC on 21 December and Paka's inner core mean rainrate are seen in Fig. 10. Paka encountered SSTs above 28° C which are greater than the critical temperatures required to support convective growth (i.e., approximately 26° C [Gray 1979]) throughout the period.

However, these SSTs were less than those that Opal (1995) traversed in the Gulf of Mexico during its lifetime (Rodgers et al. 1998; Black and Shay 1997; Shay et al. 1997). The figure also indicates an increase in the SSTs of nearly 1.0° C between 9-11 December as the system moves westward into an eddy of warm SSTs. Between 11-19 December, the SSTs initially decreased and then remained near 28.0° C. After 19 December, Paka entered a region of rapidly decreasing SSTs as it moved into the cooler ocean regions of the western North Pacific. Although SSTs were warm enough to maintain convective growth throughout the majority of the period, it is obvious that the extreme increase and decrease of SSTs between 9-11 December and after 19 December, respectively, had a profound effect on Paka's intensity.

2) MAXIMUM POTENTIAL INTENSITY

To estimate the average environmental tropopause temperature that Paka encountered during its typhoon and super-typhoon stages, the Atoll and Guam radiosonde data are used. As Paka moved to within 2° latitude south of the Kwajalein Atoll on 11 December, the mean tropopause temperature was approximately 197 K. This temperature was nearly 2° K lower than the tropical mean tropopause temperatures and 1° K lower than the mean tropopause temperature at 2° latitude radius from the center of a mean western Pacific typhoon (Frank 1976). On 15 December, when Paka passed to within 6° latitude east of Guam and prior to radiosonde failure, the mean tropopause temperature was approximately 192 K. This temperature was nearly 7° K lower than the tropical mean tropopause temperatures and 2° K lower than the mean tropopause temperature at 6° latitude radius from the center of a mean western Pacific typhoon.

Assuming that the SSTs were approximately 28° C at both locations, and that the surface air temperatures were 1°-2° C less than the SSTs, Paka's minimum potential central

pressure using Emanuel's (1985) technique at Kwajalein Atoll and Guam were between 924-935 hPa and 918-930 hPa, respectively. On the other hand, Paka's minimum central pressure near Kwajalein Atoll and Guam from the Dvorak (1974) technique and the maximum wind/minimum central pressure relationship (Ackinson and Holliday 1977), were, respectively, 965 hPa and 900 hPa. Although Emanuel's minimum potential central pressures are subject to errors due to assumptions in his technique and the uncertainties in the measured mean SSTs and tropopause temperatures that Paka encountered, these results suggest that Paka was approaching its potential intensity as it passed Guam.

3) VERTICAL WIND SHEAR

The evolution of Paka's vertical wind shear and inner core mean rainrates seen in Fig. 11 suggest that the vertical wind shear that Paka encountered before 20 December was somewhat weak (i.e., mean value of 10.7 m s^{-1}) and varied little (i.e., standard deviation of 2.1 m s^{-1}), except on 13 December when Paka passed an upper-tropospheric trough. Maximum vertical wind shear never reached values greater than 15.0 m s^{-1} prior to 20 December. Plan views of the vertical wind shear upstream of Paka (figure not shown) also indicates that the maximum vertical wind shear that Paka would have confronted 12 hours later was no greater than 12 m s^{-1}. Although these mean vertical wind shear values are slightly larger than the threshold values of 8.5 m s^{-1} that are needed to inhibit tropical cyclone intensification (Fitzpatrick 1996), it appears from the figure and earlier documented studies that Paka's vertical wind shear had little influence on its inner core rainrates during the majority of the time prior to 20 December. After 20 December, however, Paka's vertical wind shear increased to values greater than 15 m s^{-1} and this appeared to have helped reduce its mean inner core rainrates.

b Possible Sufficient Conditions That May Have Initiated and Maintained Inner Core Convective Bursts or CRB cycles

1) LOWER-TROPOSPHERIC ENVIRONMENTAL FORCING

The availability of moist air is an external forcing condition that may have helped to maintain and initiate the outer core (>333 km radius from a tropical cyclone's center) convective rainbands and CRB cycle in Paka. To examine the response of Paka's outer core rainrates to the availability of moist air, the distribution of the TPW derived from SSM/I and estimated from the ECMWF analyses at 2009 UTC on 16 December and 0000 UTC on 17 December, respectively, are shown in Fig. 12. These times roughly coincide with Paka's third convective burst.

There are two distinct results that are noted from this figure. First, it is clearly seen that the SSM/I-derived and the ECMWF-analyzed synoptic-scale TPW fields are generally similar in areal extent and magnitude. However, there are small-scale differences caused either by the differences in time and spatial resolution of the products, the lack of moisture and wind measurements used in the ECMWF analyses, and/or the inability of the SSM/I to supply TPW over land and in raining areas. Nevertheless, since the ECMWF analyzed TPW is consistent with the large-scale synoptic features observed by the SSM/Is, the plan view of the ECMWF-measured TPW fields and the mean tropospheric (i.e., 1000-400 hPa layer) and 850 hPa HMF can be used to determine the effect of the distribution of TPW on the initiation and maintenance of Paka's outer core convective burst and CRB cycle. Secondly, the TPW and 850 hPa streamline analyses reveal an intrusion of moist and dry lower-tropospheric air into, respectively, the northeastern quarter and southern half of Paka's outer core.

The evolution of Paka's outer core time- azimuthal analysis of the 850 hPa HMF (Fig. 13) indicates a large influx of water vapor that first occurred at 0600 UTC on 9 December in the northeastern quadrant of Paka. This moisture influx maintained a maximum between the 10-15 December. The influx of moisture then shifted towards the southeastern quadrant and then reintensified. This enhanced moisture influx may have been influenced by both the increased availability of moisture east and south of Paka as well as Paka's intensification.

The figure also suggests that there was a lack of moist air in Paka's southeast quadrant prior to 11 December that later shifted to Paka's northwest quadrant. The loss of moisture in the southeast and northwest quadrants appears to have been related to the dry subsiding air downstream of Paka as the typhoon's outflow converged with the basic current. After 17 December, when Paka turned more northward and began to interact with the subtropical jet, cross sectional analyses of the vertical motion and equivalent potential temperature (figure not shown) indicate that Paka's outflow converged with the westerlies, subsided, and was entrained into the western region of the tropical cyclone's outer core by the lower-tropospheric circulation. This subsiding air caused very dry air to penetrate the western periphery of Paka's outer core.

To ascertain whether the tropospheric (i.e., 1000-400 hPa layer) HMF has any influence in initiating, enhancing, or maintaining Paka's outer core rainrates and CRB cycle, the evolution of the azimuthally averaged tropospheric HMF is compared to that of the outer core mean rainrates (Fig. 14). It is seen from the figure that there was an approximate two-day cycle in the enhancement of Paka's outer core rainrate throughout the 12-day period. This was preceded one day earlier by an inward surge of moisture into Paka's outer core. These cycles in the outer core rainrates are particularly evident on 11, 13, 15, and 17 December 1997. The figure suggests that on 10 and 12 of December, the

inward surge of moisture intitated the first two episodes of increasing outer core rainrates. Then, on 14 December, the inward surge of moisture aided in the formation of the outer core convective rain band that initiated the CRB cycle, while the inward surge on 16 December enhanced and maintained the new inner core eye wall.

Another period of interest that is delineated by the figure is the time of rapid decrease in the inward surge of moisture that occured between 17-19 December. The reduction of moisture flux led to dramatically decreased moisture in the outer core and eventually in the inner core rainrates. As described earlier, the decreasing values of HMF at this time reflects strong upper-tropospheric convergence and subsidence as Paka began to interact with the westerlies (see Fig. 12). After 19 December, further inward surges of moisture occured (i.e., 20 December). Once again, this led to the enhancement of Paka's outer core rainrates, but these outer bands had little influence on the system's inner core rainrates and intensification due to the increased vertical wind shear and decreasing SSTs.

2) UPPER-TROPOSPHERIC ENVIRONMENTAL FORCING

The time-latitude distance of 150 hPa geopotential heights (Fig. 15) indicates that between 1200 UTC on 9 to 1200 UTC on 12 December an upper-tropospheric trough with heights less than 14300 m propagated southeastward and interacted with Paka. Further, the time-latitude distance of 100-200 hPa PV field (Fig. 16) within Paka's environment suggests that the tropical cyclone encounterd a region of PV-poor ascending air east of the trough axis between 0000 UTC on 11 to 0000 UTC on 12 December. During this time, a strong diffluent outflow channel west of Paka was generated (figure not shown) that appears to have helped initiate the first convective burst (Fig. 2).

After passing west of the trough axis on 12 December, Paka entered into the confluent region of the upper-tropospheric trough that contained increasing PV-rich subsiding air and vertical wind shear. These adverse conditions for tropical cyclone maintenance may have caused the rainrates in the inner core eye wall region to become steady state. As Paka continued its westward movement, the system encountered a Mid-Pacific anticyclonic vortex to the east on 13 December that intensified to the north and west of the system, and, Paka re-emerged in diffluent westerly anticyclonic outflow. This tropical cyclone/anticyclone interaction appears to have helped initiate the second inner core convective burst and lasted until 16 December when Paka once again encountered another, but weaker, upper-tropospheric trough (i.e., delineated by low upper-tropospheric PV values [Fig. 16]). After passing the second trough, Paka, once again, emerged into the favorable influence of the Mid Pacific anticyclone. As Paka continued west northwestward, it finally began to move into juxtaposition with the westerly subtropical jet on 19 December. The decreasing upper-tropospheric geopotential height fields (Fig. 15) that Paka encountered indicates that Paka was moving out of the influence of the supporting Mid-Pacific ridge and into the hostile westerlies.

Figure 17, which depicts the evolution of Paka's upper-tropospheric eddy relative angular momentum flux that was azimuthally averaged for an annulus 600-1000 km from Paka's center and mean inner core rainrate, suggests that during the majority of the time the upper-tropospheric outflow surrounding the system had a negative influence on Paka's growth by diverging relative angular momentum away from the system. The only times when ERFC was observed was on 9 December and prior to the time when Paka interacted with the second (16 December) upper-tropospheric trough. However, the maximum magnitudes of the ERFC were no greater than 5 m s^{-1} day^{-1}, considerably less than the critical value of 10 m s^{-1} day^{-1} that is observed for moderate environment-tropical cyclone interaction (DeMaria et al., 1993).

However, in examining the time-radial view of the azimuthally mean 200 hPa ERFC surrounding Paka (Fig. 18) it is clearly seen that during the periods prior to the first and second inner core convective bursts there is an inward surge of upper-tropospheric eddy relative angular momentum originating from Paka's environment (<444 km radius from the center). During the interaction with the first upper-tropospheric trough, the inward surge of eddy relative angular momentum approached the inner core, while during the interaction with the weaker second trough, the inward surge of eddy relative angular momentum only reached to within 500 km of the center. Thus, the figure suggests that the influx of eddy relative angular momentum into the inner core during the first upper-tropospheric trough interaction, although negative within the larger annular area, may have had greater influence in enhancing the rainrates in the inner core eye wall region than it had during the interaction with the second trough.

7 Summary and discussion

It has been clearly demonstrated that between 9-21 December, the large oscillations in tropical cyclone Paka's rainrate/LHR caused by three long lasting inner core convective bursts and one CRB cycle has been sufficiently captured using the combination of SSM/I and TMI sensor data. The analyses also indicate that the convective burst prior to and particularly during the CRB had a profound effect on Paka's intensification.

For example, the first episode of inner core convective burst that occurred on 10 December helped to intensify Paka to typhoon status, where Paka's maximum winds increased from 22 ms^{-1} to 58 ms^{-1} in a two day period (see Fig. 2). The second convective burst occurred between 13-14 December after a slight decrease in rainrates and appeared, once again, to help reintensify Paka. On 15 December, an outer convective rainband

formed, propagated inwards, and increased in rainrate. This outer rain band dissipated the original eye wall by decreasing its water vapor influx and subjected the system to increasing upper-tropospheric subsidence. This caused a momentarily weakening of the system. By 16 December, the new outer convective rainband helped reintensify Paka's maximum winds. After the new inner core eye wall reached its minimum radius and maximum rainrates on 18 December, the third convective burst reintensified Paka to a maximum strength of nearly 80 ms^{-1}. Finally, as Paka moved further into the westerlies, its rainrates and intensity decreased under the influence of increasing vertical wind shear, the intrusion of dry air, and decreasing SSTs.

During these inner core convective bursts cycles, the satellite-derived rainrates/LHR observations suggest the following: 1) rainrates increased; 2) convective processes dominated in the generation of latent heat; 3) large net latent heating penetrated deeper layers of the troposphere; 4) the eye wall propagated closer to the center of circulation; 5) eye wall became more symmetric; and 6) eye wall became more electrically charged. Because of these convective bursts, the distribution and intensity of latent heating may have helped intensify tropical cyclone Paka by generating enough buoyancy to compensate for the loss of the eye wall cyclonic angular momentum due to surface friction and upper-tropospheric outward transport. Due to deep layer latent heating, the eye wall cyclonic angular momentum (i.e., a function of eye wall radius and symmetry) was able to concentrate the upper-troposphere warming nearer to the center of circulation. Further, if one considers the reduction of atmospheric density with height, the higher the warming occurs, the lower the surface pressure could be reduced hydrostatically at the center of Paka's circulation, and the more intense the tropical cyclone could become.

Since Paka occurred over the data void ocean regions of the central and western North Pacific, the poor spatial and temporal resolution of the ECMWF analyses, and the

non-coincidence of model analyses and satellite observations made it difficult to assess the cause and effect relationship between actual internal forcing mechanisms and those estimated from the satellite data. Nevertheless, if one only emphasizes the significant forcing mechanisms, the results of this study suggest that convective bursts were mainly supported by the ideal necessary conditions, and to a lesser extent initiated by the sufficient conditions for convective growth.

For example, in examining the necessary conditions for convective growth the results indicate that: 1) Paka's environmental thermodynamic conditions were ideal for the system to reach its maximum potential intensity (MPI) during the later stages of its evolution. These favorable conditions were dictated by the high SSTs, the elevated height and cold temperatures of the tropopause, and the abundance of available moisture. 2) The vertical wind shear during 9-19 December was slightly greater than the critical values of 8.5 ms^{-1} that have been shown to be adverse for convective growth. 3) The SSTs were consistently 2.0° C above the threshold of value 26° C during this period, a criterion that has been shown to be necessary for the extraction of enough surface heat flux to provide for convective growth. The warm SSTs were particularly favorable for generating the first convective burst on 10-11 December, when Paka encountered a warm eddy of SSTs that was 2.5° C warmer than the threshold value.

The apparent sufficient conditions, on the other hand, suggest: 1) Prior to the first convective burst, Paka traversed the diffluent region of a minor upper-tropospheric trough on 10-11 December as it encountered the warm pool of SSTs. Although the diffluent outflow was observed, the outflow generated ERFC that reached the inner core was less than what was needed for moderate tropical cyclone/trough interaction. However, the combination of the warm ocean eddy and the weak influx of eddy relative angular momentum may have been sufficiently strong to help initiate and maintain the first

convective burst. 2) During the second convective burst, as Paka emerged from the confluent region of the upper-tropospheric trough and into Mid-Pacific ridge, the inner core rainrates increased slowly, reaching steady state on 12 December. This convective burst appeared to initiate a second period of intensification. 3) From the 13-20, as Paka entered the CRB cycle that helped initiate the third convective burst on 17 December, the tropical cyclone remained under the influence of the Mid-Pacific ridge; 4) After 20 December, stronger vertical wind shear, lower SSTs, and greater intrusion of dry air began to erode the new inner core eye wall and eventually weakened Paka (see Fig 2). 5) Finally, the inward surge of moisture that occurred in the southeastern quadrant and the loss of moisture that occurred in the southwestern quadrant of Paka's outer core regions may have, respectively, helped to initiate and dissipate these convective bursts and CRB cycle.

As in Opal (Rodgers et al. 1998), Paka's latent heat distribution and intensity greatly influenced its intensity. However the sufficient environmental forcing conditions that helped initiate and maintain Paka's convective burst were not as strong as those found in tropical cyclone Opal. Paka was generally more intense than Opal, but Paka's lower-tropospheric HMF convergence values were only about half as large as Opal's and the values of upper-tropospheric ERFC were less than the critical value of 10 m s^{-1} day^{-1} and were considerably less than those observed during Opal's mature stage. Paka's weaker sufficient environmental forcing conditions were most likely due the system's low latitudinal development within the Mid-Pacific ridge that protected the system from most upper-tropospheric troughs. The results also suggest that Paka's necessary conditions were ideal for intensification and that the periods of convective burst were more internally forced (i.e., CRB cycles) in contrast to external forcing that is found in higher latitude systems. As suggested in the Opal case and more strongly emphasized in this case, the distribution and intensity of inner core latent heating needs to be monitored more often in order to better forecast tropical cyclone intensity changes. This might be accomplished by

assimilating remotely sensed latent heat data into a three-dimensional meso-scale numerical weather prediction models.

Acknowledgements: The authors wish to thank Stacy Stewart of NOAA Tropical Prediction Center for his contribution in the synoptic analyses, Christopher Velden of the Space Science and Engineering Center at the University of Wisconsin for supplying the GMS infrared observations, and Dr. Robert Adler of Code 912 NASA/Goddard Space Flight Center for his support and critique of this paper. The study was supported by NASA Headquarters Dynamics and Thermodynamic Research Program headed by Dr. Ramesh Kakar.

APPENDIX A

a Geostationary Meteorological Satellite (GMS)

Since there are no reconnaissance flights, Paka's best track intensity measurements (maximum sustained surface wind speeds and minimum central surface pressure) are estimated from the 11.5 um channel of the Japanese geosynchronous satellite GMS infrared sensor by employing the Dvorak (1974) scheme. However, Gaby et al. (1980) determined that the Dvorak technique tended to underestimate the tropical cyclone maximum winds by approximately 5 kts in the middle North Atlantic as compared to the HURDAT (Hurricane Data) file. The HURDAT file primarily uses reconnaissance flight data in the region of the middle North Atlantic. Another problem with the Dvorak scheme was that it constrains the 24 hour pressure falls by approximately 50 hPa, which sometimes makes the tropical cyclone intensity spin-up and spin-down time inaccurate. Nevertheless, since this study is more interested in intensity change, rather than absolute intensity, the weakness of the Dvorak scheme should have little impact in this study.

The study also uses the GMS infrared sensor to estimate Typhoon Paka's inner core mean CDO T_{BB} for the purpose of qualitatively verifying whether SSM/I and TMI-observations are frequent enough to capture the major temporal changes in Paka's mean rainrates and to monitor Paka's eye size. The water vapor (6.7 um) channel of the GMS infrared sensor is used to monitor qualitatively the propagation of the middle and upper-tropospheric waves, while the water vapor-derived winds are employed to help derive a more accurate upper-tropospheric wind analyses around Paka.

b Earth Probe Total Ozone Mapping Spectrometer (TOMS)

The Earth Probe borne TOMS was launched July 1996 and provided daily total ozone information for Paka from 14-21 December 1997. TOMS uses the solar backscatter of six ultraviolet wavelengths from 312.5 to 380.0 nm to separate the effects of cloud and ground reflection, scattering, and ozone absorption, thereby determining total ozone in a vertical column. TOMS measures total ozone at local noon with a nadir IFOV of approximately 50 km Total ozone is measured in Dobson units (DU), where 1000 DU equals 1 atm cm. In cloudy regions, where ozone below the clouds are not observed, total ozone measurements are corrected by adding a climatological profile of tropospheric ozone below a cloud at a given height. The fraction of cloud cover is obtained from the TOMS ultraviolet reflectivity measurements (i.e., 380.0 nm radiance) and the cloud height is based on climatology (i.e., International Satellite Cloud Climatology Project (ISCCP) data set. The ISCCP data was averaged monthly over a 0.5° latitude X 0.5° longitude grid (McPeters et al. 1996).

Over deep clouds that are associated with tropical cyclones, the underestimation of cloud height may cause a 2% underestimation in the TOMS-observed total ozone amount.

However, these deep convective clouds are also highly reflective, which enables the TOMS to observe more backscattering ultraviolet radiation as compared to the low reflective ocean surfaces (Fishman et al. 1987). The high reflectivity of the cloud would cause TOMS to observe more total ozone and, thereby, possibly compensate for the loss of total ozone caused by the underestimation of the cloud height. Therefore, clouds should not bias the estimation of the relative spatial distribution of TOMS-derived total ozone observation.

To eliminate the longitudinal and particularly the latitudinal total ozone gradients, fields, the TOMS total ozone anomaly measurements are used. Total ozone anomalies are obtained from the Earth Probe TOMS data by subtracting the Nimbus-7 TOMS-derived climatology values of total ozone for a given day and location (based on 15 years of Nimbus-7 TOMS measurements) from the observed Earth Probe TOMS data.

These measurements are used to help monitor and justify the upper-tropospheric circulation surrounding tropical cyclone Paka. By examining the mutual adjustment between upper-tropospheric waves and tropical cyclone outflow (Rodgers et al. 1990), it has been demonstrated that the distribution of total ozone reflects the distortion of the tropopause and PV fields caused by strong three-dimensional transport processes that are associated with upper-tropospheric waves, the secondary circulation induced by subtropical and tropical cyclone outflow jets, and the eye regions in tropical cyclones.

c Lightning derived from Optical Transient Detector (OTD) satellite

The OTD is used to examine the evolution of the distribution of lightning in tropical cyclone Paka and to help identify convectively active regions. The OTD observes an area 1300 X 1300 km twice a day with a viewing time of 189 seconds and a spatial resolution of 15 X 15 km area. However, there can be a location error as high as 30 km due to

navigation errors. The OTD monitors an oxygen emission line a 777.4 um to detect intracloud and cloud to ground lightning. It detaches the optical pulses associated with the dissociation and excitation of oxygen due to lightning. The day and night flash detection efficiency is estimated to be roughly 50%. Approximately, 10% of the flashes detached by OTD is false due to radiation, electronic noise, or solar glint.

Due to detection efficiency, short view time, and the navigational errors, there is a limit of the OTD's ability to monitor low flash rates that are common in tropical cyclones (Cecil and Zipser (1998). Nevertheless, the OTD observation will be used to augment the TRMM LIS lightning detection.

d TRMM Lightning Imaging Sensor (LIS)

The TRMM LIS instrument is an optical starring telescope and filter imaging system. It monitors the distribution and variability of both cloud-to-cloud and cloud-to-ground lightning. LIS also measures at the frequency .777 um and has a spatial resolution of approximately 4 - 7 km over a 600 X 600 km swath of the earth's surface. Due to the TRMM orbit, LIS can observe a cloud region for almost 90 seconds as it passes overhead, which is long enough to estimate the flashing rate of most electrical storms. The instrument records the time of occurrence, measures the radian energy, and determines the location of lightning events within its IFOV. For more information concerning the LIS sensor and measurements may be found in Christian et al. (1992).

APPENDIX B

a Upper-tropospheric environmental parameters and cross sectional analyses

The 150 hPa geopotential heights (m), horizontal divergence fields (s^{-1}), and streamlines and the 100 and 200 hPa layer PV (10^{-7} mb $s^{=1}$) analyses are derived for the purpose of examining Paka's upper-tropospheric environmental circulation. Northwest-southeast cross sectional analyses through Paka's are also constructed in order to examine the vertical distribution of the total wind flow and the potential temperatures within Paka and its environment. Tropopause temperatures, on the other hand, are obtained from Kwajalein Atoll and Guam prior to and during Paka and combined with the mean SSTs to qualitatively derive the system's MPI.

b Vertical wind shear

Vertical wind shear is considered for its ability to hinder convective growth (Gray 1979; Rueter and Yau 1986; Mundell 1991). It has been shown (DeMaria and Huber 1998) that vertical wind shear can negatively effect tropical cyclone structure and intensity through either ventilation caused by differential advection of heat, by the generation of a secondary circulation caused by the movement of a vertically coherent vortex, or by tilting and stabilization of its vortex caused by the thermal adjustments that are required to maintain balance as the PV vortex becomes titled.

The vertical wind shear (m s^{-1}) is derived from the 850 and 200 hPa ECMWF wind analyses. Horizontal winds at the 850 and 200 hPa level are averaged over a 500 km^2 circular domain centered on the tropical cyclone. The tropical cyclone vortex is not removed. The large domain is used to assure a more accurate vertical wind shear analyses over the relatively data-void central and western North Pacific region where Paka occurred. The vertical wind shear is then estimated from the magnitude of the difference between the mean horizontal wind vectors at 850 and 200 hPa. The vertical wind shear is also

generated upstream of Paka, for the purpose of estimating the magnitude of the vertical wind shear that the tropical cyclone would encounter 12 to 24 hours later.

c Upper-tropospheric horizontal eddy relative angular momentum flux convergence (ERFC)

In order to monitor the influence at which the gradient winds adjustment process that is associated with Paka's outflow alters the system's inner core LHR; Paka's upper-tropospheric horizontal ERFC (m s^{-1} day^{-1}) is examined. The upper-tropospheric horizontal ERFC was calculated in Lagrangian cylindrical coordinates (Molinari and Vollaro 1989; DeMaria et al. 1993) using the following equation:

$$ERFC = -r^{-2}\frac{\partial}{\partial r}(r^2\overline{v_r' v_\theta'}) \qquad (1)$$

where r is the radius from the tropical cyclone center, V_r is the radial wind and V_θ is the tangential wind. The over-bar represents an azimuthal average and the prime denotes the deviation from the azimuthal average (e.g. eddy term). The radial and tangential winds in Lagrangian coordinates are obtained from the 200 hPa ECMWF wind analyses. The ERFC values are azimuthally averaged within an annulus whose inner and outer radii are, respectively, 600-1000 km from Paka's center. To delineate the inward surge of eddy relative angular momentum into Paka, the upper-tropospheric ERFC is also calculated for annuli whose width are 50 km that extends 100 to 900 km from Paka's center. The data is presented as time-radius analyses.

d Mean tropospheric horizontal moisture flux (HMF)

Some of the physical processes that have allowed the lower-tropospheric to influence tropical cyclone Paka's rainrate/LHR, have been documented to be the surface evaporation (Frank 1977) and the strong horizontal surges of low-level water vapor convergence (Ooyama 1964; Charney and Eliassen 1964: Molinari and Scubis 1985; Lee 1986). For this study, the mean tropospheric horizontal moisture flux (HMF) is examined in Lagrangian cylindrical coordinates in order to ascertain what effects the inward surges of water vapor has on altering, the precipitation rates within Paka's inner and outer core regions.

The mean tropospheric HMF (10^8 kg s^{-1}) was again calculated in Lagrangian cylindrical coordinates (Frank, 1977) by using the following equation:

$$HMF = \frac{2\pi r}{g} \int_P \overline{V_r q}\ dP \qquad (2)$$

where r is the radius from the tropical cyclone center, q is the mixing ratio, V_r is the radial wind velocity, g is gravity, dP is a vertical pressure increment, and P is the pressure level of integration. The over-bar represents an azimuthal average. The radial winds and mixing ratio are obtained from the ECMWF analyses at mandatory levels up to 300 hPa. The mean tropospheric moisture flux is calculated for a cylindrical volume whose radius is 333 km from Paka's center of circulation and between the pressure levels of 1000 and 300 hPa. The cylindrical radius of 333 km is chosen for the following reasons: 1) the analysis is comparable to the resolution of the ECMWF analyses; 2) the lower- and middle-tropospheric wind observations are more abundant outside of the central dense overcast region; and 3) earlier water vapor budget studies indicated that the water vapor flux contributed more to the total precipitation within this circular area than surface evaporation (Frank, 1977). Because of the uncertainties of measuring sea surface evaporation and the fact that not all water vapor convergence contributes to precipitation production, there is no

attempt to relate the changes in the water vapor budget to variations in the inner core LHR. The evolution of the azimuthal distribution of the 850 hPa water vapor flux (the level at which maximum water vapor flux is usually found) is also calculated from the ECMWF analyses in order to determine the asymmetry of the influx of water vapor with time.

REFERENCE

Ackinson, G. D. and C. R. Holiday, 1977; Tropical cyclone minimum sea level pressure/maximum sustained wind relationship for the western North Pacific. *Mon. Wea. Rev.*, **105**, 421-471.

Black, P. G., and L. K. Shay; 1998: Observation of tropical cyclone intensity change due to air-sea interaction processes. Preprints, *Symposium on Tropical Cyclone Intensity Change* Amer. Meteor Soc., 11-16 January 1998, Phoenix Arizona pp. 161-168.

Baik, J-J., S-M Lee, and C.H. Cho, 1993: Examination of convective process representation and inertial stability in a tropical cyclone model. *J. Korean Meteor.*, **28**, 308-323.

Challa, M. and R. Pfeffer, 1980: Effects of eddy flux of angular momentum on model hurricane development. *J. Atmos. Sci.*, **37**, 1603-1618.

Charney, J. G. and A. Eliassen, 1964: On the growth of the hurricane depression. *J. Atmos. Sci.*, **21**, 68-75.

Chen, L. and W. M. Gray, 1985: Global view of the upper level outflow patterns associated with tropical cyclone intensity changes during FGGE. Colorado State University, Atmospheric Science Paper, 392, 1216 pp.

Cecil, D. J. and E. J. Zipser, 1998: Relationships between tropical cyclone intensity and satellite-based indicators of inner core convection: 85-Ghz ice-scattering signature and lightning. *Mon. Wea. Rev.*, **127**, 103-123.

Christian, H. J., R. J. Blakeslee, and S. J. Goodman, 1992: Lightning imaging sensor (LIS) for the earth observing system, NASA TM-4350. Available from Center for Aerospace Information, P.O. Box 8757, Baltimore Washington International Airport, Baltimore, MD 21240, 44 pp., 1992.

Delden, A. van., 1989: On the deepening and filling of balanced cyclones by diabatic heating. *Meteor. Atmos. Phys.*, **41**, 127-145.

DeMaria, M. J-J. Baik, J. Kaplan, 1993: Upper level eddy angular momentum fluxes and tropical cyclone intensity change. *J. Atmos. Sci.*, **50**, 1183-1147.

DeMaria, M, and J. Kaplan, 1994: A statistical Hurricane intensity prediction scheme (SHIPS) for the Atlantic Basin. *Wea. Forecasting,* **9**, 209-220.

De Maria M., and M. M. Huber, 1998: The effects of vertical shear on tropical cyclone intensity change: An historical perspective. Preprints, *Symposium on Tropical Cyclone Intensity Change*, Amer. Meteor Soc., 11-16 January 1998, Phoenix, Arizona pp. 22-29.

des Jardins, M., K. Brill, and S. Schots, 1991: Use of GEMPAK on Unix Workstations. Preprints. *Seventh Int. Conf. on Interactive Information and Processing Systems for Meteorology, Oceanography, and Hydrology*, New Orleans, LA., Amer. Meteor. Soc. 449-451.

Dvorak, V. F., 1975: Tropical cyclone intensity analyses and forecasting from satellite imagery. *Mon. Wea. Rev.*, **103**, 420-430.

Emanuel, K.A., 1993: An air-sea interaction theory for tropical cyclones. Part 1: Steady-state maintenance. *J. Atmos. Sci.*, **43**, 585-604.

Frank, W. M., 1977: The structure and energetics of the tropical cyclone. Part 1: Storm structure. *Mon. Wea. Rev.*, **105**, 1119-1135.

Fishman, J. and J. C. Larsen, 1997: Distribution of total ozone and stratospheric ozone in the tropics. Implication for the distribution of tropospheric ozone. *J. Geosphys. Res.*, **92**, 6627-6634.

Fitzpatrick, P. J., 1996: Understanding and forecasting tropical cyclone intensity change. Colorado State University, Atmospheric Science Paper 598, 346 pp.

Gaby, D. C., J. B. Sushine, R. M. Mayfield, S. C. Pearce, and F. E. Torres, 1980: Satellite classification of Atlantic tropical and subtropical cyclones: A review of eight years of classification at Miami. *Mon. Wea. Rev.*, **108**, 587-595.

Gray, W. M., 1979: Hurricanes: Their formation, structure, and likely role in the tropical circulation. *Meteorology over the Tropical Oceans.* D. B. Shaw, Ed. Roy. Meteor. Soc., 155-218.

Hollinger, J. O., 1991: DMSP Special Sensor Microwave/Imager calibration/validation. Final Report Vol. 11, 1225 [Available from the author at Naval Research Laboratory, Washington, D.C., 20375].

Kummerow, C., W. S. Olson, and L. Giglio, 1996: A simplified scheme for obtaining precipitation and vertical hydrometeor profiles from passive microwave sensors. *IEEE Trans. Geosci. Remote Sensing,* **34,** 1213-1232.

Kummerow, C., W. Barnes, T Kozu, 1. Shine, and J. Simpson, 1998: The Tropical Rainfall Measuring Mission (TRMM) sensor package. *J. Atmos. Oceanic. Technol,* **15,** 809-817.

Lee, C. S., 1986: An observational study of tropical cloud cluster evolution and cyclogenesis in the Western North Pacific. Colorado State University, Atmospheric Science Paper 403, 250 pp.

Lyons, W. A., and C. S. Reed, 1994: Observations of lightening in convective supercells within tropical storms and hurricanes, *Mon. Wea. Rev.*, **122,** 1897-1916.

McPeters, R. D., S. M. Hollandsworth, L, E. Flynn, J. R. Herman, and C. J. Seltor, 1996: Long-term ozone trends derived from the 16-year combined Nimbus-7/Meteos 3 TOMS Version 7 Record. *Geophys. Res. Lett.*, **23,** 3099-3702.

Marks, F. D. 1985: Evolution of the structure of precipitation in Hurricane Allen (1980). *Mon. Wea. Rev.*, **113,** 909-930.

Marks, F. D. and R. A. Houze, 1987: Inner-core structure of Hurricane Alicia from airborne doppler radar observations. *J. Atmos Sci.*, **44,** 1296-1317.

Merrill, R. T., 1988: Environmental influence on hurricane intensification. *J. Atmos. Sci.*, **45,** 1678-1687.

Molinari, J., P. K. Moore, V. P. Idome, R. W. Henderson, and A. B. Saljoughy, 1994: Cloud-to-ground lightening in Hurricane Andrew. *J. Geophy. Res.*, **99**, 16665-16676.

Molinari, J. and S. Skubis, 1985: Evolution of the surface wind field in an intensifying tropical cyclone. *J Atmos. Sci.*, **42**, 2865-2879.

Molinari, J. and D. Vollaro. 1989: External influences on hurricane intensity. Part 1: Outflow layer eddy momentum fluxes, *J. Atmos. Sci.*, **46**, 1093-1105.

Molinari, J., K. P. Moore, V P. Idone, 1988: Convective Structure of hurricanes as revealed by lightning locations. *Mon. Wea. Rev.*, **127**, 520-634.

Morales, C. A., J. S Kriz. E. B. Rodgers, and J. A. Weinman, 1997: The evolution of sferics around hurricane Lilli (1996), Preprints, 22 Conf. on Hurricanes and Tropical Meteorology, Fort Collins, Co., Amer. Meteor. Soc., 127-128.

Mundell, D. B., 1991: Tropical cyclone intensification. Preprints, *19th Conf. Hurricanes and Tropical Meteorology,* Miami, FL., Amer. Meteor. Soc., 511-515.

Olson, W. S., C. D. Kummerow, G. M. Heymsfield, and L. Giglio, 1996: A method for combined passive-active microwave retrievals of cloud and precipitation profiles. *J. Appl. Meteor.*, **35**, 1763-1789.

Olson W. S., C. D. Kummerow, Y. Hong, and W.-K. Tao, 1999: Atmospheric latent heating distributions in tropics derived from satellite passive microwave radiometer measurements. *J. Appl. Meteor.*, **38**, 633-664.

Ooyama, K. V., 1964: A dynamical model for the study of tropical cyclone development. *Geifus, Int.*, **4**, 187-198.

Orville R. E., R. A. Weisman, R. B. Pyle, R. W. Henderson, and R. E. Orville, 1987: Cloud-to-ground lightning flashes characteristics from June 1994 through May 1995. *J. Geophys. Res.* **92**, D5 5640-6544.

Petty, G. W., and K. B. Katsaros, 1990: New geophysical algorithms for the Special Sensor Microwave Imager. Preprints. *Fifth Int. Conf. on Satellite Meteorology and Oceanography*, London, England, Amer. Meteor. Soc., 247-251.

Reed, R. J., A. Hollingsworth, W. A. Heckle, and F. Dell, 1988: An evaluation of the performance of the ECMWF operational system in analyzing and forecasting easterly wave disturbances over Africa and tropical Atlantic. *Mon. Wea. Rev.*, **116**, 824-865.

Rodgers, E. B., J. Stout, J. Steranka, and S. Chang, 1990: Tropical cyclone-upper-atmospheric interaction as inferred from satellite total-ozone observations. *J. Appl. Meteor.*, **29**, 933-954.

Rodgers, E. B., S. W. Chang, J. Stout, J. Steranka, and J-J. Shi, 1991: Satellite observations of variations in tropical cyclone convection caused by upper-tropospheric troughs. *J. Appl. Meteor.*, **30**, 1163-1184.

Rodgers, E. B., S. W. Chang, and H. F. Pierce, 1994a. A satellite observational and numerical study of the precipitation characteristics in western North Atlantic tropical cyclones. *J. Appl. Meteor.* **33**, 129-139.

Rodgers, E. B., J-J. Baik, and H. F. Pierce, 1994b. The environmental influence on tropical cyclone precipitation. *J. Appl. Meteor.*, **33**, 573-593.

Rodgers, E.B. and H. F. Pierce, 1995: Environmental influence on Typhoon Bobbie's precipitation distribution. *J. of Appl. Meteor.*, **34**, 2515-2532.

Rodgers, E. B., W. S. Olson, V. M. Karyampudi, and H. F. Pierce, 1998: Satellite-derived latent heating distribution and environmental influences in hurricane Opal (1995). *Mon. Wea. Rev.*, **126**, 1229-1247.

Reuter, G. W. and M. K. Yau, 1986: Numerical modeling of cloud development in a shear environment. *Bettr. Phys. Atmos.*, **66**, 65-80.

Shaw, D. B., P. Lonnberg, A. Hollingsworth, and P. Unden, 1987: Data Assimilation: The 1984/1985 revisions of the ECMWF mass and wind analysis. Quart. *J. Roy. Meteor. Soc.*, **113**, 533-566.

Shay, L. K.., O. G. Black, A. J. Mariano, J. D. Hawkins, and R. L. Exlberry, 1992: Upper ocean response to hurricane Gilbert. *J. Geophy. Res.*, **97**, 20227-20248.

Shi, J-J., S. W. Chang, and S. Raman, 1990: A numerical study of the outflow layer of tropical cyclones. *Mon. Wea. Rev.*, **118**, 2042-2055.

Simpson, J., Ed. 1988: Report of the Science Steering Group for a Tropical Rainfall Measurement Mission (TRMM). U. S. Gov't Printing Office, 94 pp.

Simpson, J., C. Kummerow, W-K Tao, and R. F. Adler, 1996: On the Tropical Rainfall Measurement Mission (TRMM). *Meteor. Atmos. Phys.*, **60**, 19-36.

Weatherford, C., 1987: Typhoon structural evolution. Preprints. *17th Conf. on Hurricanes and Tropical Meteorology*, Miami, FL, Amer. Meteor. Soc., 337-340.

Willoughby, H. E., J. A. Clox, and M. G. Shoreibah, 1982: Concentric eye-walls, secondary wind maxima, and the evolution of the hurricane vortex. *J. Atmos. Sci.*, **39**, 395-411.

Willoughby, H. E., 1988: The dynamics of the tropical cyclone core. *Aust. Meteor. Mag.*, **36**, 183-191.

Willoughby, H. E., 1990: Temporal changes of the primary circulation in tropical cyclones. *J. Atmos. Sci.*, **47**, 242-264.

FIGURE CAPTIONS

Fig. 1 Best track location and intensity (see legend) for tropical cyclone Paka between 8-22 December 1997.

Fig. 2 Paka's intensity (dashed line, ms^{-1}) and SSM/I (open circle) and TMI (X)-derived mean total (i.e., combined stratified and convectively generated rainrates) inner core (within 111 km of the center) rainrates (solid line, mmh^{-1}) for the period between 9-21 December 1997.

Fig. 3 Paka's SSM/I/TMI-derived mean total inner core rainrates (solid line, mmh^{-1}) interpolated for every six hours and the size of the eye (dashed line, km) determined from GMS IR data for the period between 9-21 December, 1997.

Fig. 4 Paka's SSM/I/TMI-derived mean total inner core rainrates (solid line, mmh^{-1}) interpolated for every six hours and the mean inner core cloud top T_{BB} (K) determined from GMS IR data for the period between 9-21 December, 1997.

Fig. 5 Paka's SSM/I/TMI-derived inner core mean total (solid line, mmh^{-1}) and convective generated rainrates (dashed lines, mmh^{-1}) interpolated for a six hours interval during the period between 9-21 December 1997.

Fig. 6 Time-radius view of Paka's azimuthally averaged SSM/I/TMI-derived convective generated rainrates (contours of rainrate are shown in figure and given in mmh^{-1}) interpolated for every six hours and six hour maximum winds (ms^{-1}) for the period between 9-21 December, 1997. Rainrates were azimuthally averaged for annuli 55 km in

width extending 444 km outwards from the center. The greatest rainrates are delineated by the warmest colors.

Fig. 7 Plan view of Paka's convectively generated rainrates (mmh^{-1}) from the SSM/I and TMI observations at 0509 UTC on 13, 0831 UTC on 14, 0817 and 2149 UTC on 15, and 1435 UTC and 2243 UTC on 16 December, 1997 during Paka's CRB cycle. Gray background is non-raining SSM/I/TMI observations, while the colors indicated rainrates of different intensities (see color bar). Radial rings are 1° latitude interval centered on Paka's center.

Fig. 8 A radial-height display of the azimuthally averaged SSM/I/TMI-derived total LHR ($W\ m^{-3}$) for the same CRB cycle seen in Fig. 7. Latent heating was azimuthally averaged for annuli 55 km in width extending 333 km outwards from the center. Non-colored regions (i.e., regions of negative latent heating) indicate a loss of latent heat due to evaporation. Contour interval is given in the figure. The darker the colors, the greater the latent heating.

Fig. 9 A plan view of Paka's CDO regions (Paka's eye delineated by a darker shade point within the CDO) obtained from a GMS IR image at 1832 UTC on 12 December, 1997 superimposed upon the OTD (white background cross) and LIS (no background cross) observed lightning strokes during the 12 December.

Fig. 10 Paka's SSM/I/TMI-derived total (solid line) inner core rainrates (mmh^{-1}) interpolated for every six hours and the 12-hour interval SSTs (°C) for the period between 9-21 December 1997.

Fig. 11 Paka's SSM/I/TMI-derived total (solid line) inner core rainrates (mmh^{-1}) interpolated for every six hours and the 12-hour interval vertical wind shear (ms^{-1}) for the period between 9-21 December 1997.

Fig. 12 The SSM/I-observed (left panel) total precipitable water (TPW, mm) and the ECMWF-derived (right panel) TPW and 850 mb winds for the environment surrounding Paka at approximately 2200 UTC on 16 December, 1997. White dot designates Paka's center. Contour intervals of TPW are given by color bar. Black in SSM/I observations are the raining areas where TPW can not be observed from this sensor.

Fig. 13 A time-azimuthal display of Paka's outer core (i.e., greater than 333 km from the center) ECMWF-derived 850 hPa HMF ($g\ kg^{-1}\ m\ s^{-1}$) for the 8-21 December. 1997. Contours of HMF are given in the figure. The darker shades delineate the larger HMF values.

Fig. 14 Paka's SSM/I/TMI-derived azimuthally averaged total (solid line) outer core rainrates ($mm\ h^{-1}$) interpolated for a six hour interval and the 12 hour interval total (integrated between 1000-400 hPa) moisture flux (HMF, $10^5\ kg\ s^{-1}$) at the radius of 333 km from Paka's center for the period between 9-21 December, 1997. Rainrates were averaged over an annulus whose outer and inner radius are 333 km and 265 km. Shaded regions delineate negative HMF values.

Fig. 15 Time-latitude distance view of the 150 hPa geopotential heights (m) that Paka traversed during the period of 9-21 December, 199&. Distance perpendicular to best track path of Paka (delineated by thick black line) are in positive and negative degrees of latitude depending, respectively, on whether one moves to the right or left of Paka direction

of motion. Contours are given in figure. Darker shades designate higher geopotential heights.

Fig. 16 Time-latitude distance view of the `100-200 hPa potential vorticity (PV, 10^{-7} mb s^{-1}) that Paka traversed during the period of 9-21 December, 199&. Distance perpendicular to best track path of Paka (delineated by thick black line) are in positive and negative degrees of latitude depending, respectively, whether one moves to the right or left of Paka direction of motion. Contours are given in figure. Darker shades designate higher PV values.

Fig. 17 Paka's SSM/I/TMI-derived total (solid line) inner core rainrates (mmh^{-1}) interpolated every six hours and the 12 hour interval azimuthally averaged 200 hPa eddy relative angular momentum flux convergence (ERFC, m s^{-1} day^{-1}) for the period between 9-21 December, 1997. ERFC was azimuthally averaged over an annulus whose outer and inner radius are, respectively, 1000 and 600 km from the center of Paka. Shaded regions delineate regions of eddy relative angular momentum flux divergence.

Fig. 18 Time-distance view of the azimuthally averaged 200 hPa ERFC (m s^{-1} day^{-1}) for the period between 9-21 December 1997. ERFC is azimuthally averaged over annuli whose widths are 100 km that extends outward form Paka's center from 100 km to 1000 km. Contours are given in figure. Darker shades designate higher ERFC values.

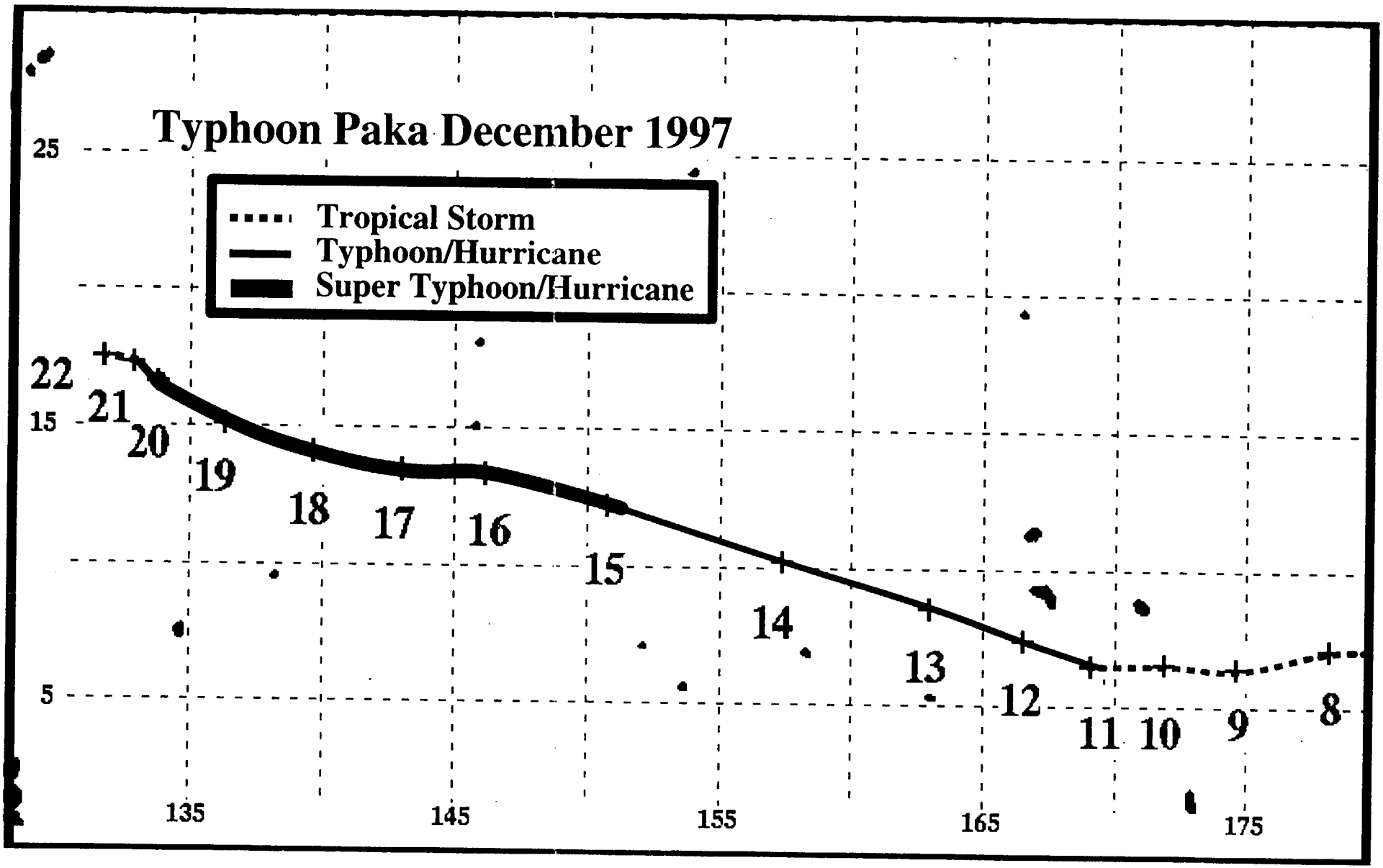
Typhoon Paka December 1997
Tropical Storm
Typhoon/Hurricane
Super Typhoon/Hurricane
25
15
5
135
145
155
165
175
22
21
20
19
18
17
16
15
14
13
12
11
10
9
8

Fig. 1

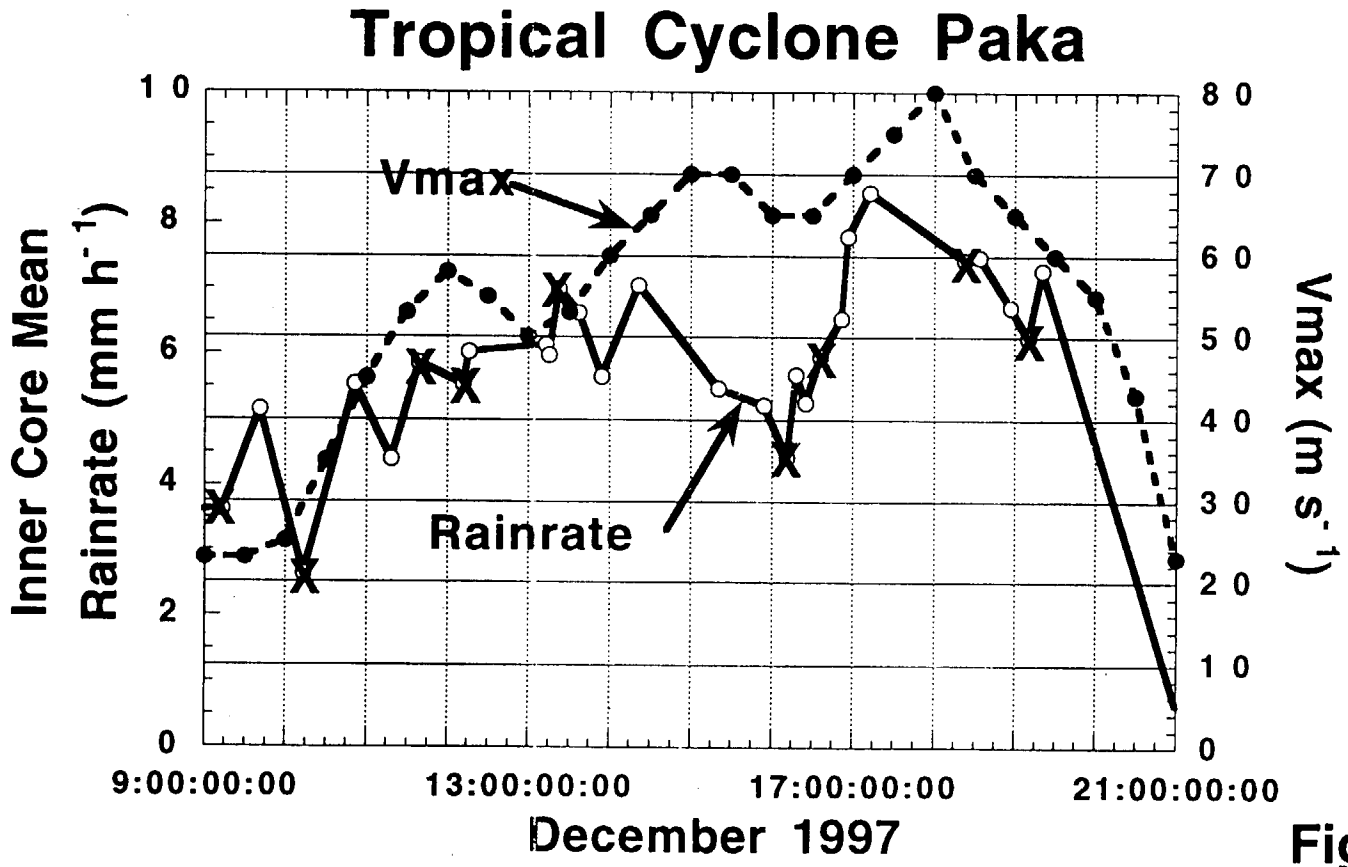
Tropical Cyclone Paka
Inner Core Mean Rainrate (mm h-1)
Vmax (m s-1)
Vmax
Rainrate
10
8
6
4
2
0
80
70
60
50
40
30
20
10
0
9:00:00:00
13:00:00:00
17:00:00:00
21:00:00:00
December 1997

Fig. 2

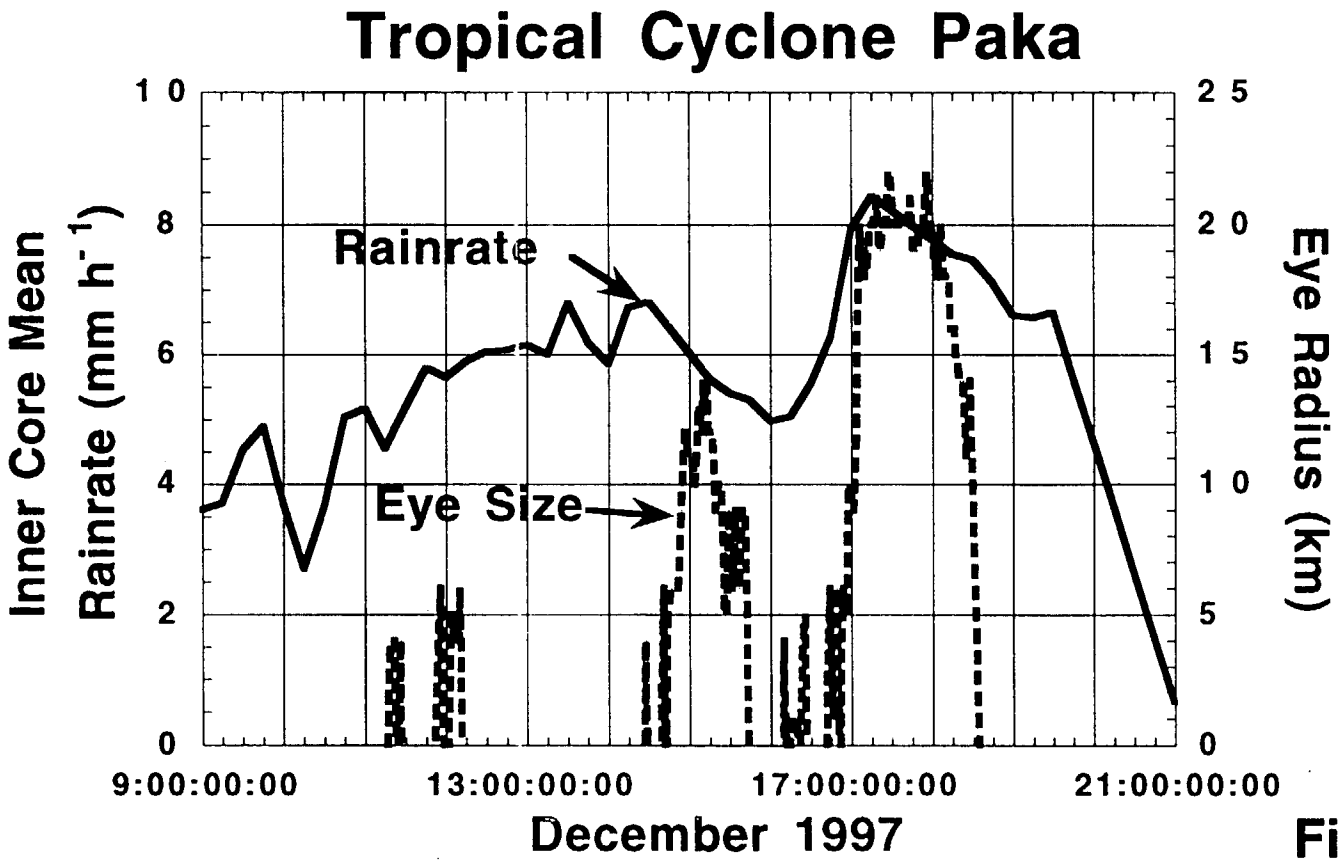
Tropical Cyclone Paka
Inner Core Mean
Rainrate (mm h-1)
Eye Radius (km)
Rainrate
Eye Size
10
8
6
4
2
0
25
20
15
10
5
0
9:00:00:00
13:00:00:00
17:00:00:00
21:00:00:00
December 1997

Fig. 3

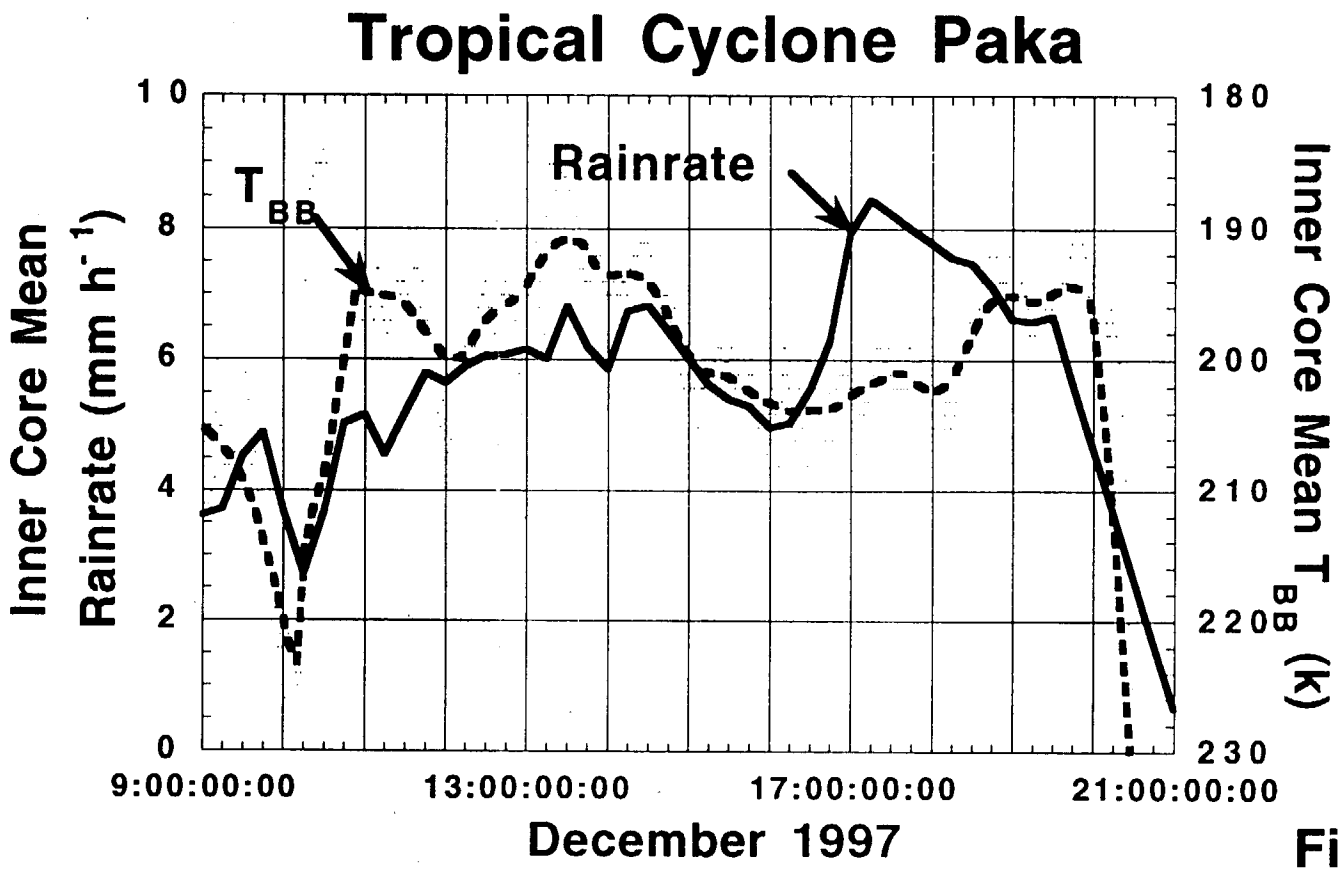
Tropical Cyclone Paka
Inner Core Mean Rainrate (mm h-1)
Inner Core Mean TBB (k)
TBB
Rainrate
10
8
6
4
2
0
180
190
200
210
220
230
9:00:00:00
13:00:00:00
17:00:00:00
21:00:00:00
December 1997

Fig. 4

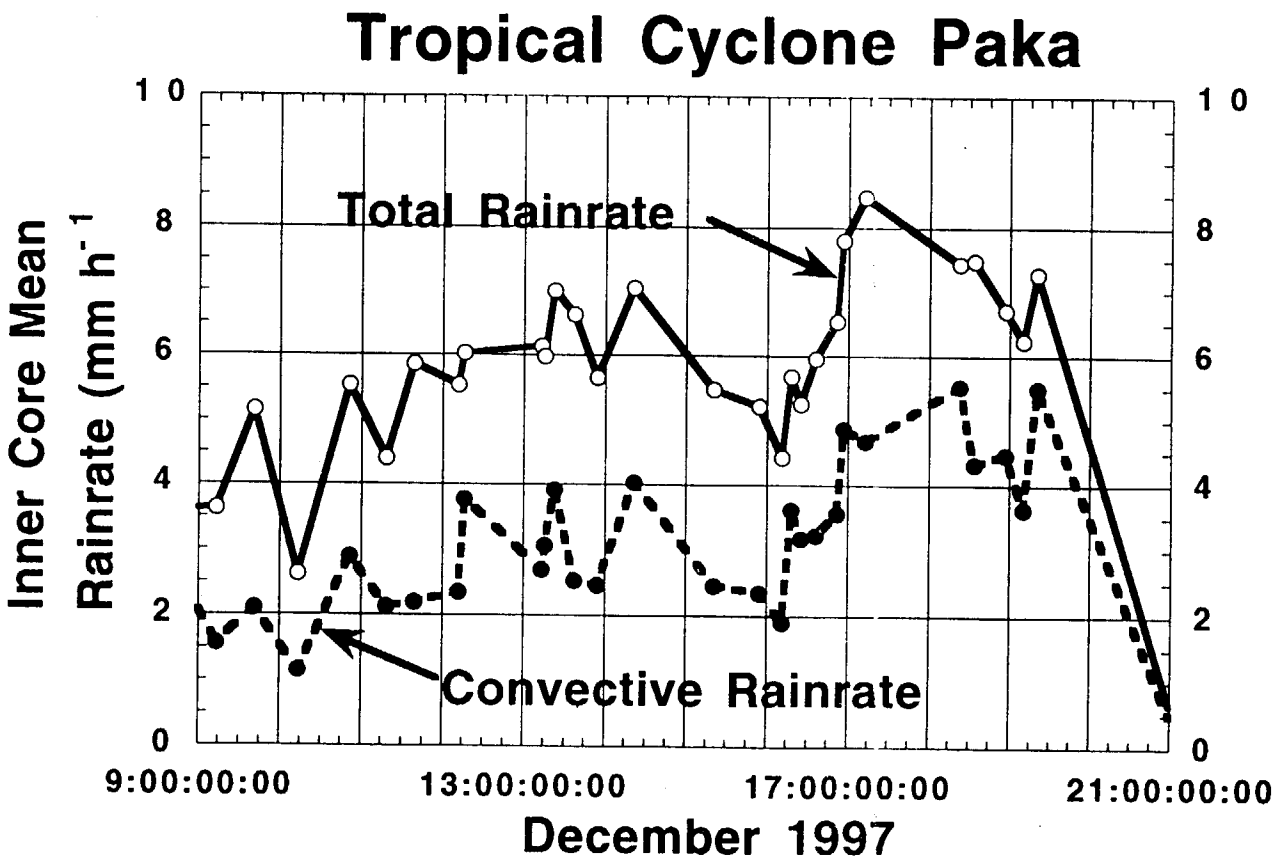
Tropical Cyclone Paka
Inner Core Mean
Rainrate (mm h-1)
10
8
6
4
2
0
Total Rainrate
Convective Rainrate
9:00:00:00
13:00:00:00
17:00:00:00
21:00:00:00
December 1997

Fig. 5

Tropical Cyclone Paka

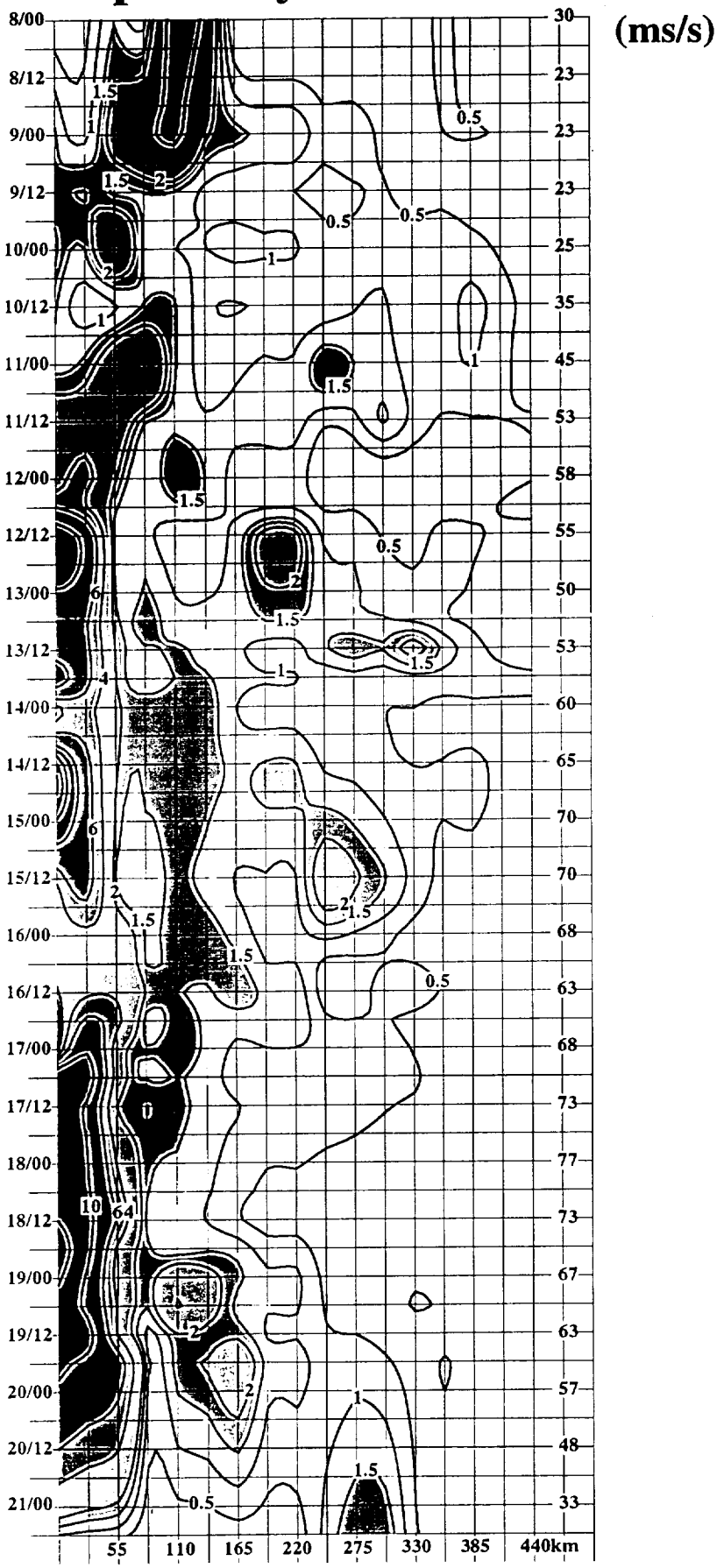

Fig. 6

Typhoon Paka

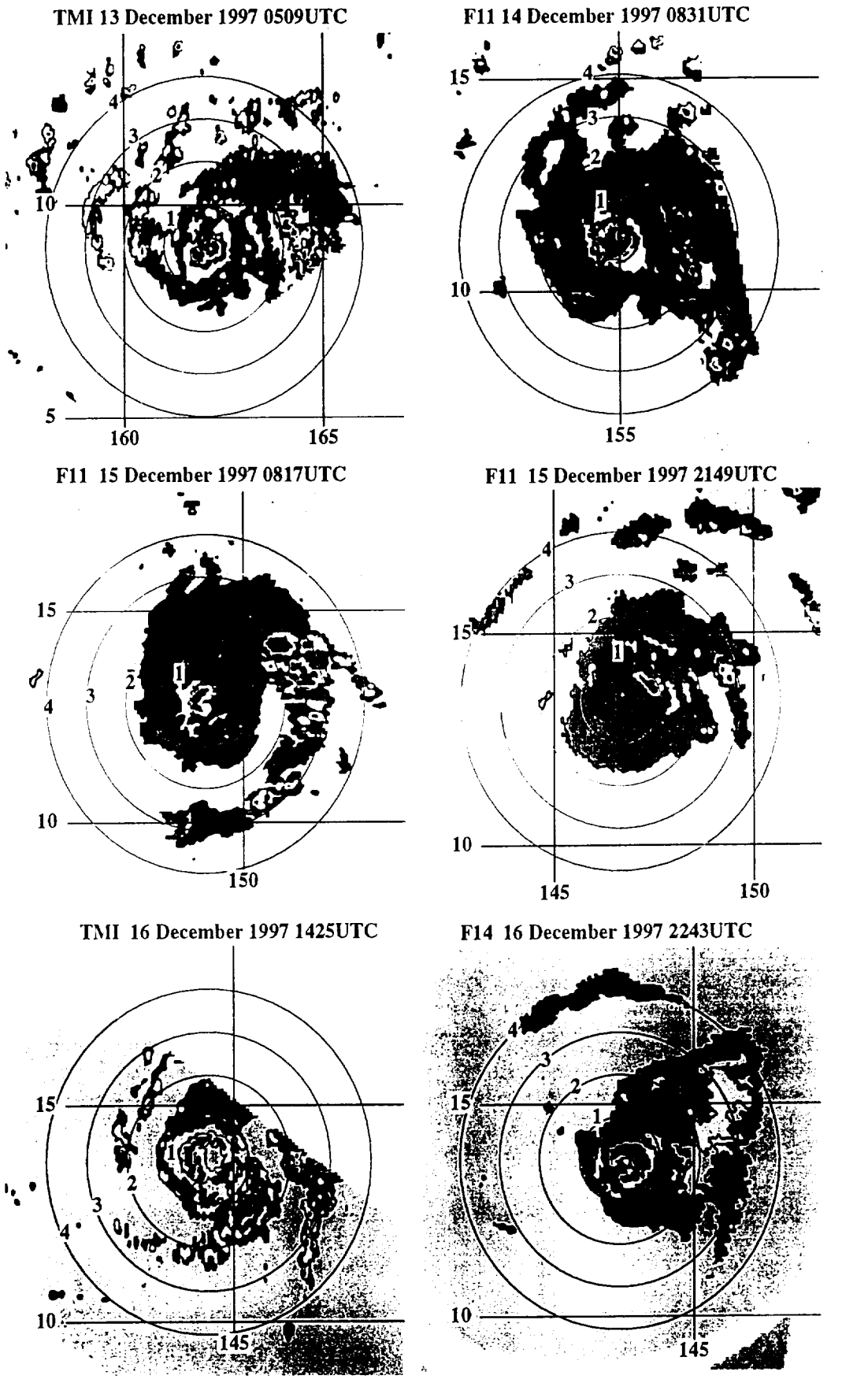

Fig. 7

Typhoon Paka

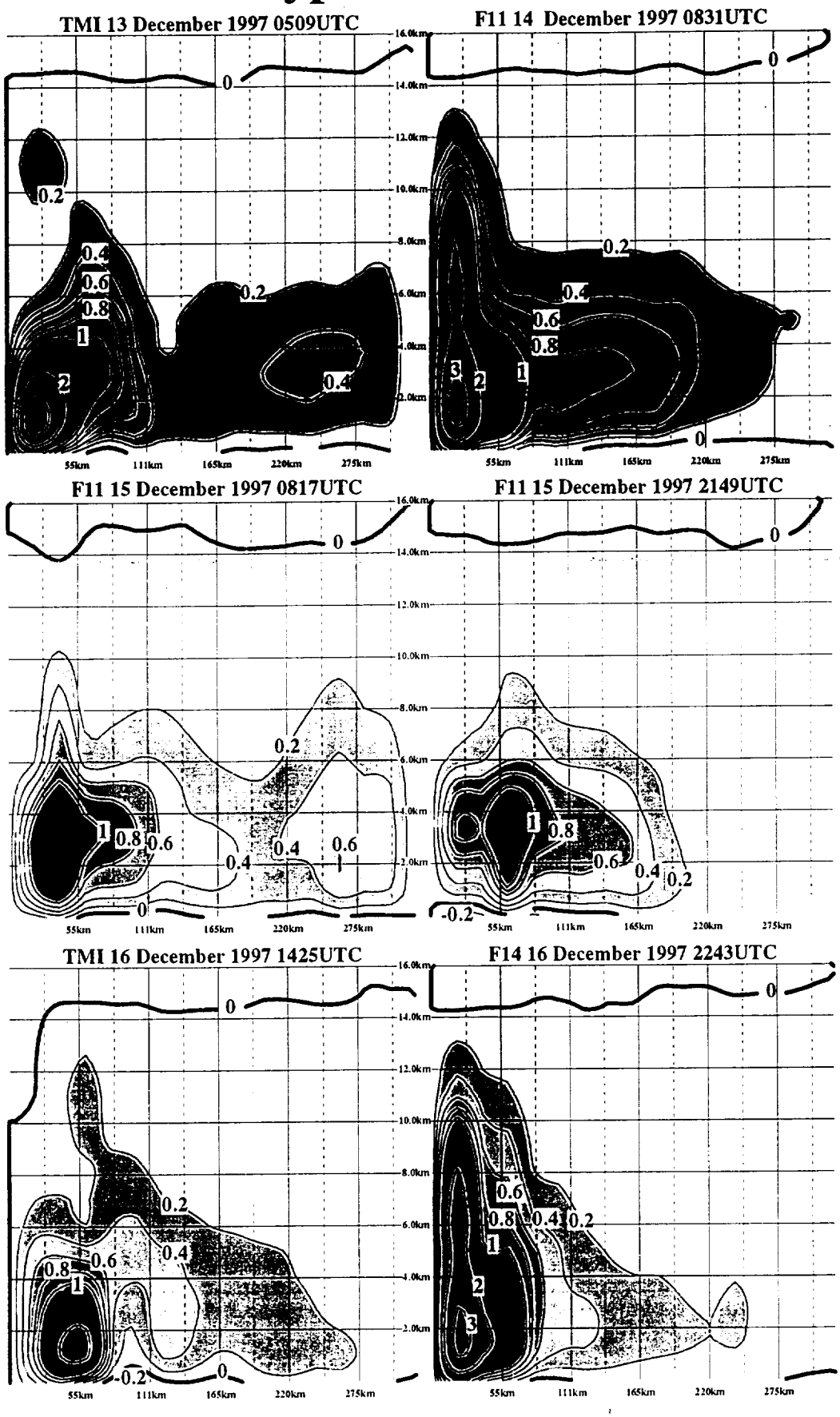

Fig. 8

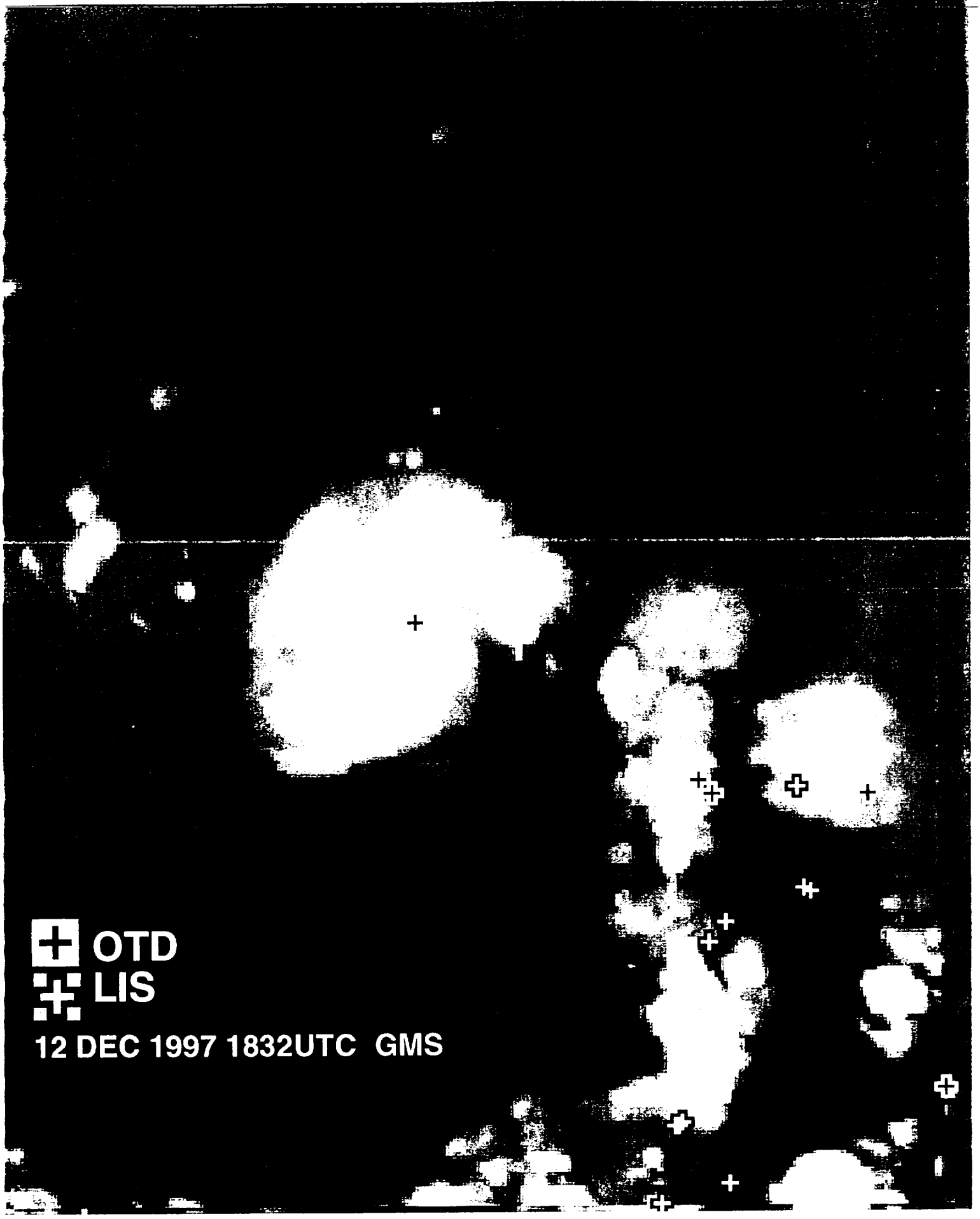

Fig. 9

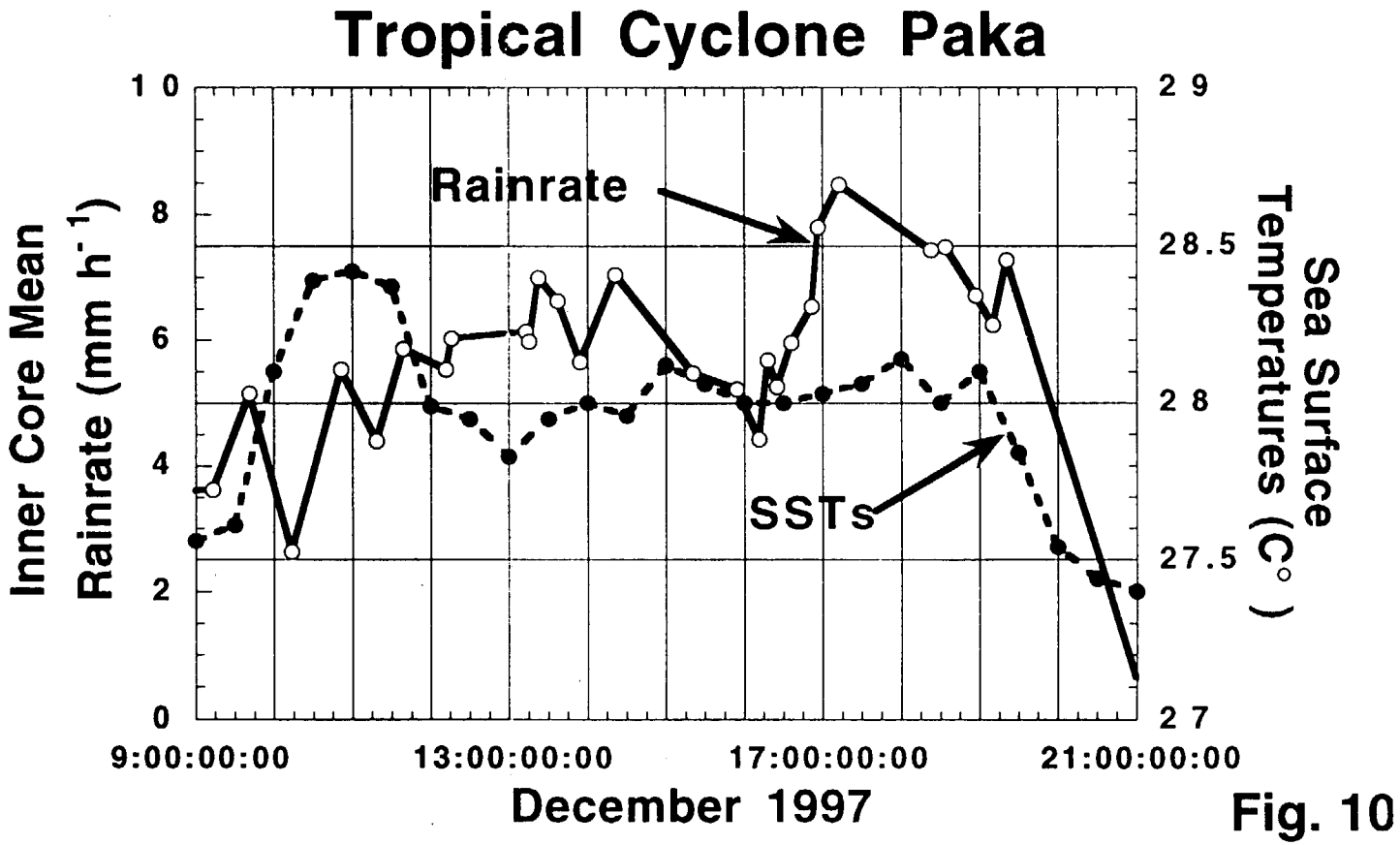
Tropical Cyclone Paka
Inner Core Mean Rainrate (mm h-1)
Sea Surface Temperatures (C°)
Rainrate
SSTs
10
8
6
4
2
0
29
28.5
28
27.5
27
9:00:00:00
13:00:00:00
17:00:00:00
21:00:00:00
December 1997

Fig. 10

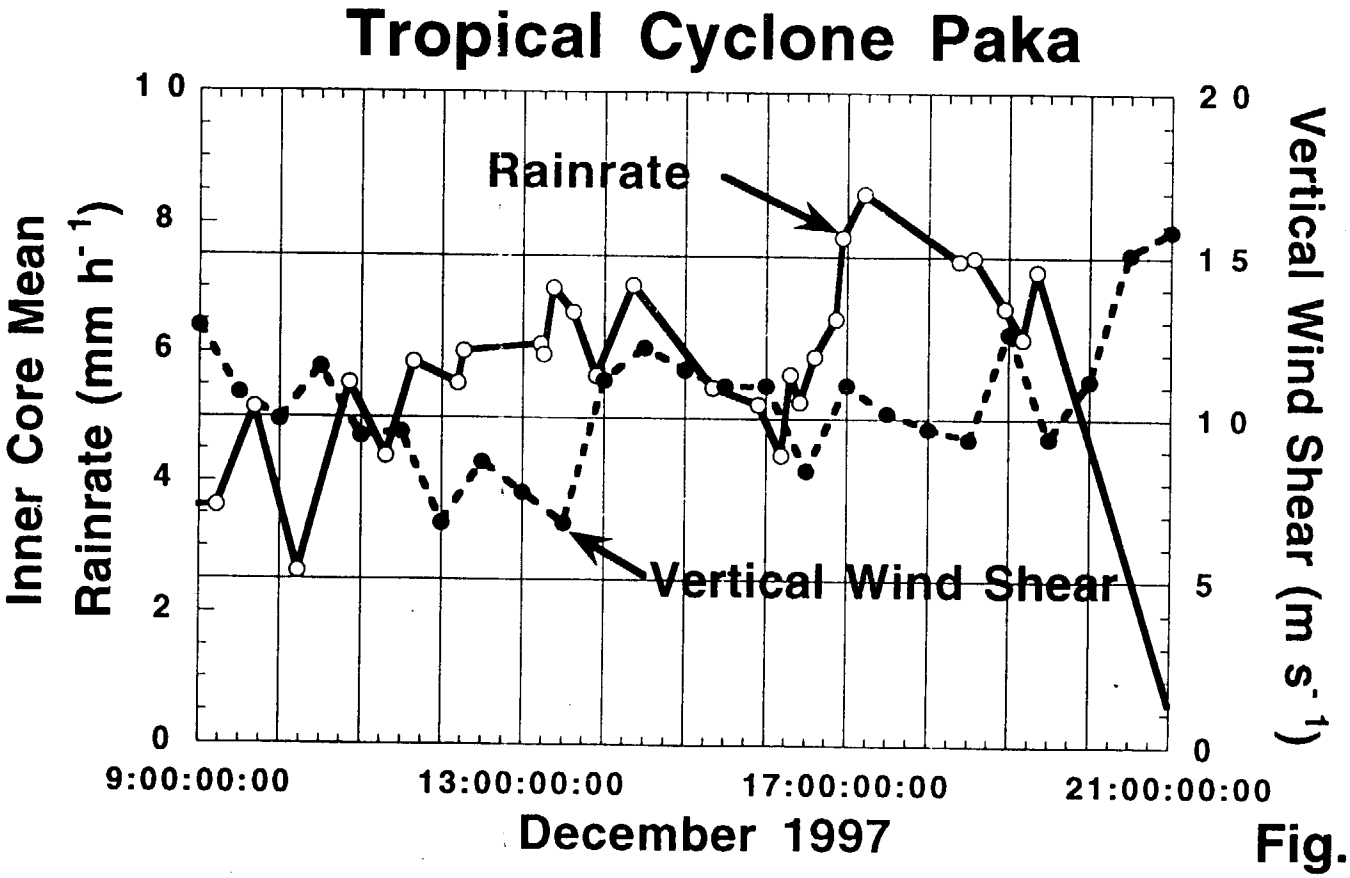
Tropical Cyclone Paka
Inner Core Mean
Rainrate (mm h-1)
Vertical Wind Shear (m s-1)
Rainrate
Vertical Wind Shear
10
8
6
4
2
0
20
15
10
5
0
9:00:00:00
13:00:00:00
17:00:00:00
21:00:00:00
December 1997

Fig. 11

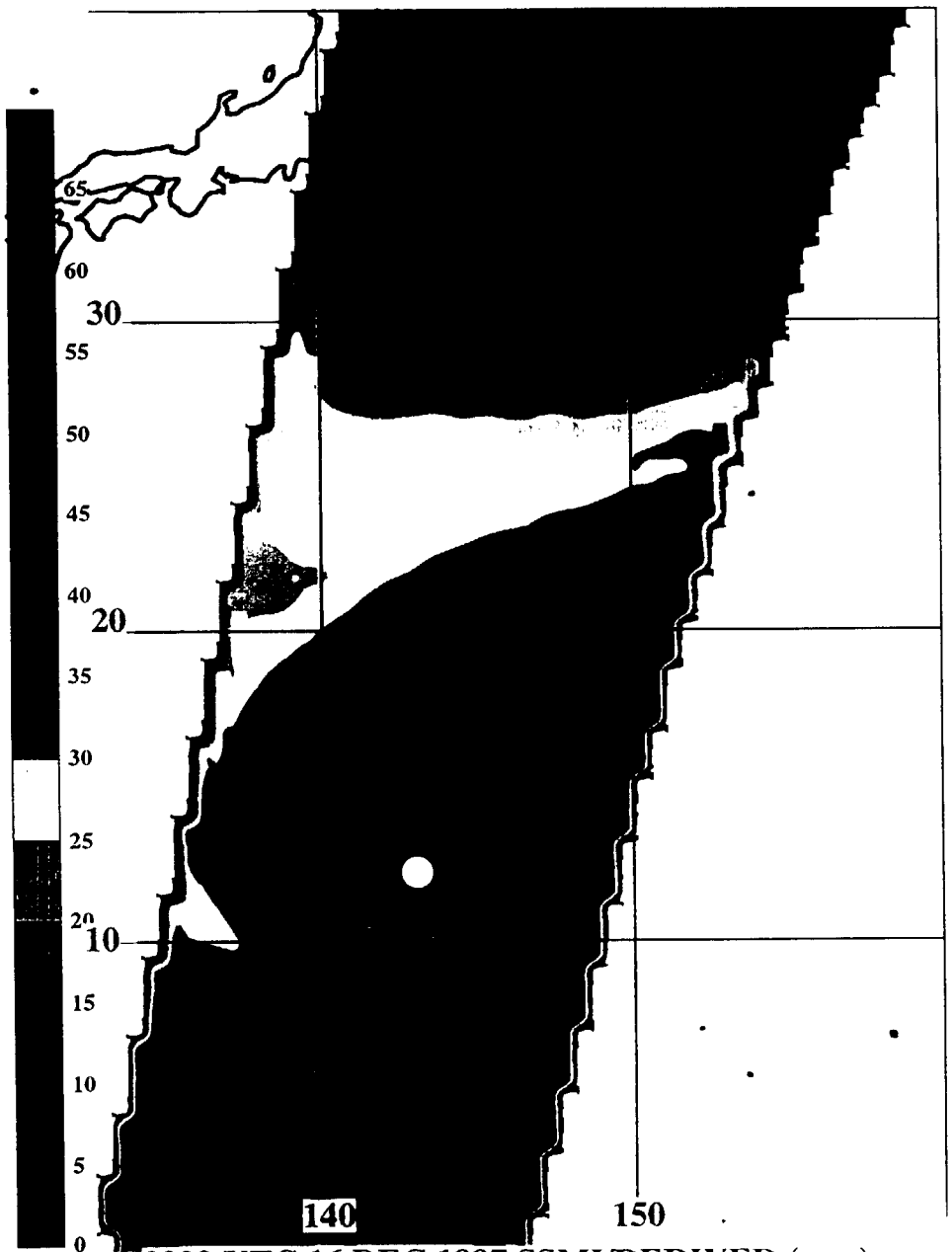

2009 UTC 16 DEC 1997 SSMI/DERIVED (mm)

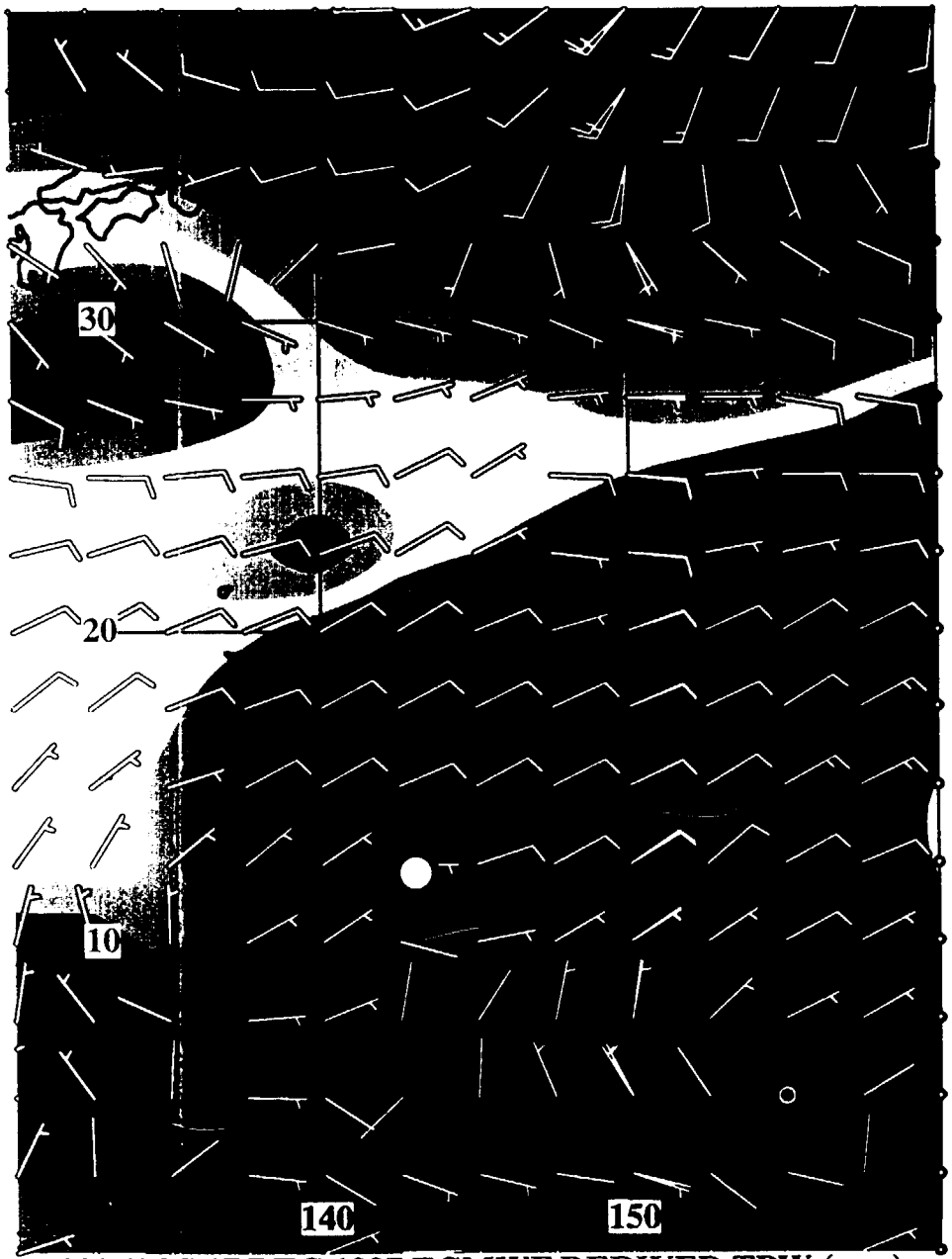

0000 UTC 17 DEC 1997 ECMWF DERIVED TPW (mm)
WITH 850MB WIND ANALYSIS

Fig. 12

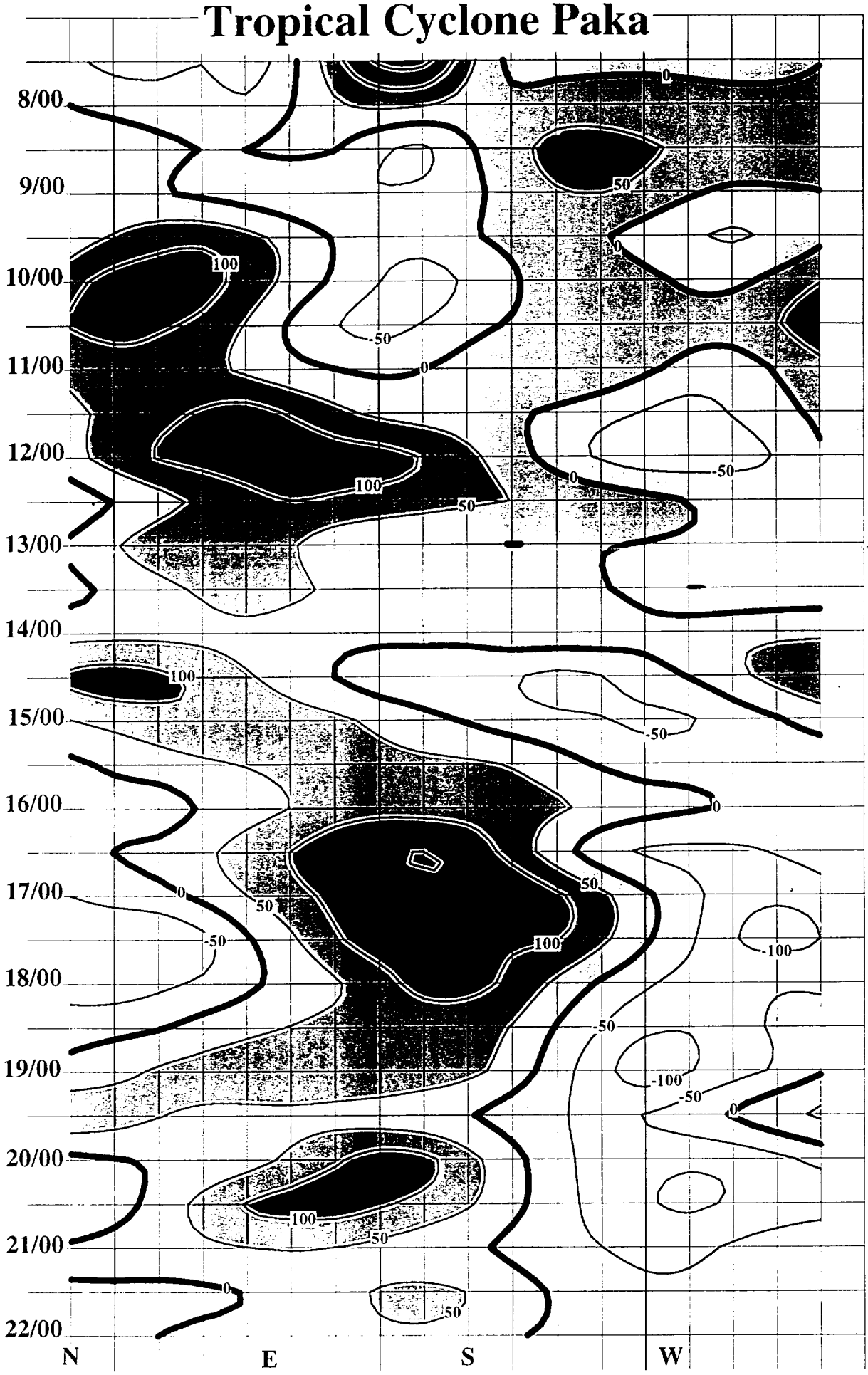
Tropical Cyclone Paka
8/00
9/00
10/00
11/00
12/00
13/00
14/00
15/00
16/00
17/00
18/00
19/00
20/00
21/00
22/00
N
E
S
W
100
50
0
-50
-100

Fig. 13

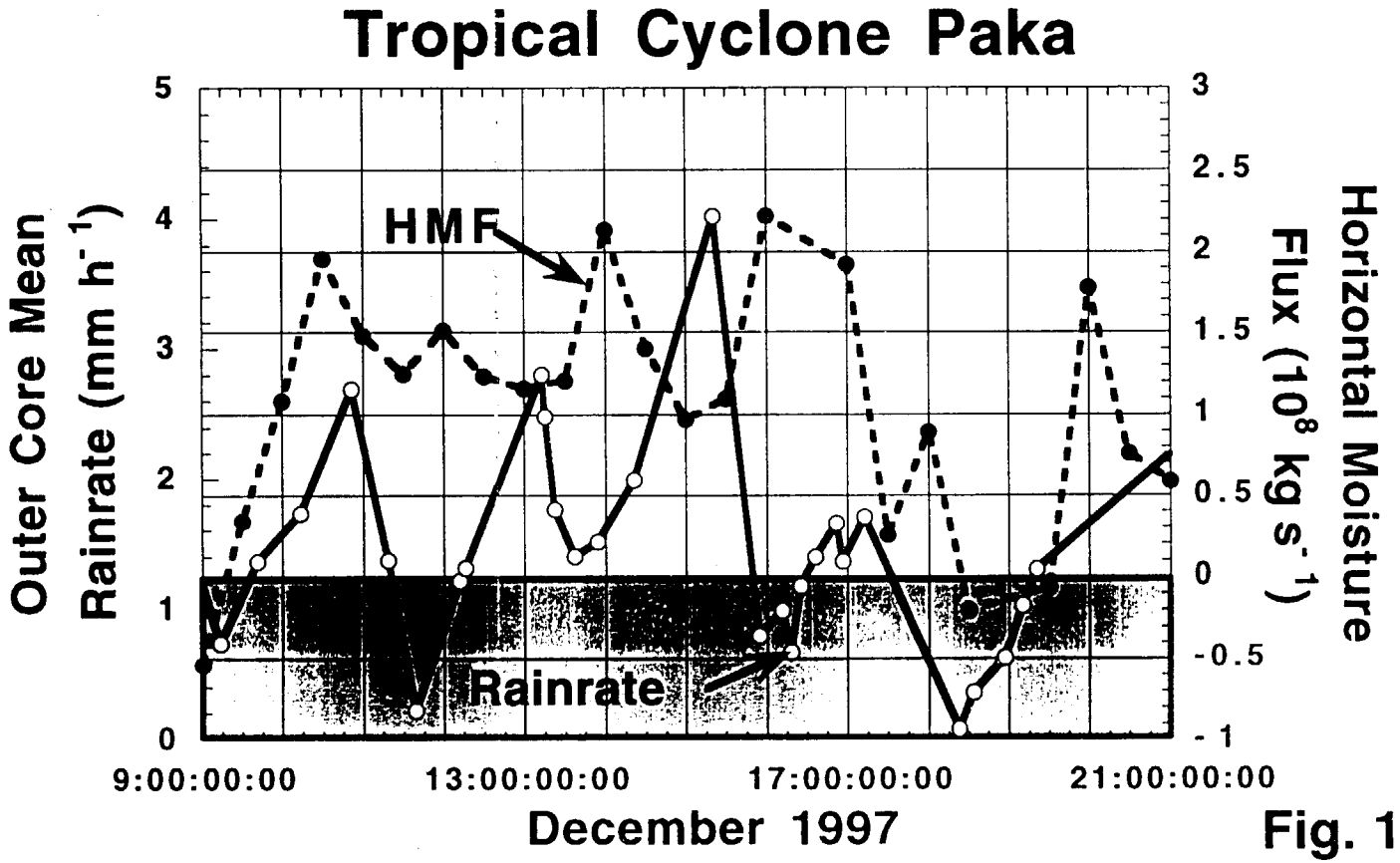
Tropical Cyclone Paka
Outer Core Mean Rainrate (mm h-1)
Horizontal Moisture Flux (10^8 kg s-1)
HMF
Rainrate
5
4
3
2
1
0
3
2.5
2
1.5
1
0.5
0
-0.5
-1
9:00:00:00
13:00:00:00
17:00:00:00
21:00:00:00
December 1997

Fig. 14

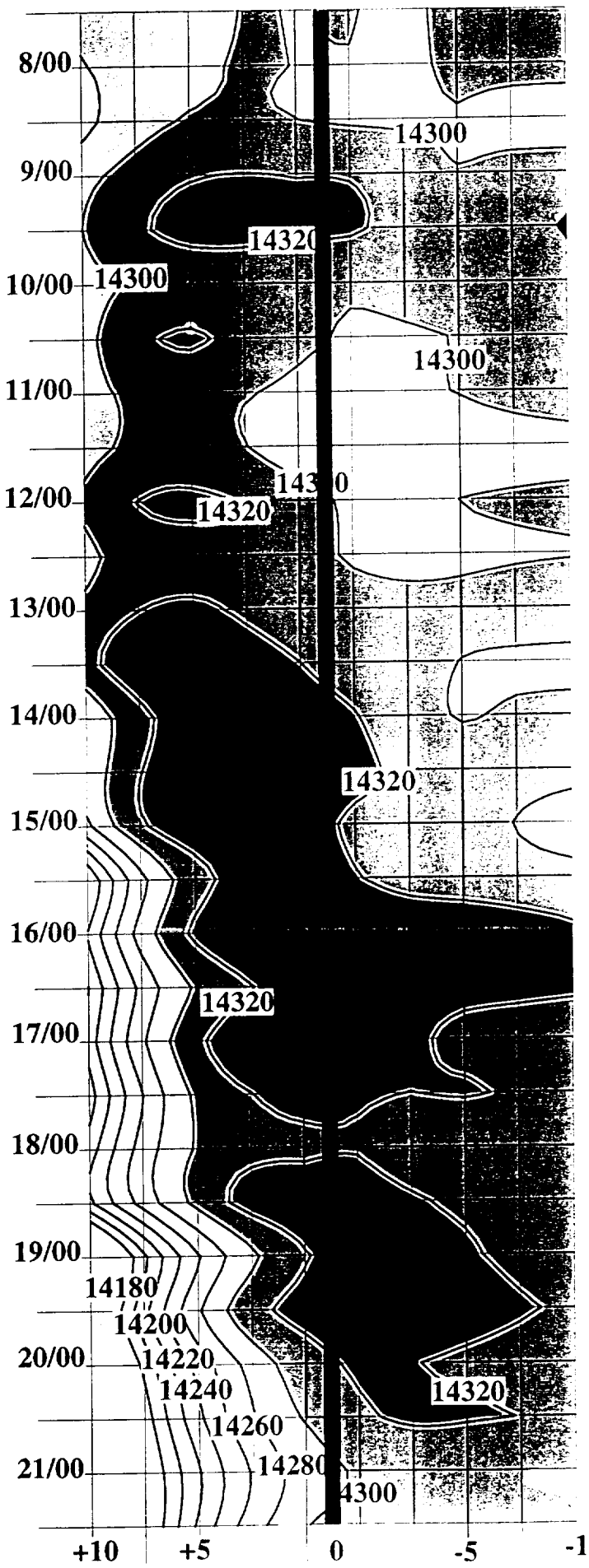
Tropical Cyclone Paka
8/00
9/00
10/00
11/00
12/00
13/00
14/00
15/00
16/00
17/00
18/00
19/00
20/00
21/00
14300
14320
14300
14300
14320
14320
14320
14180
14200
14220
14240
14260
14280
14320
+10
+5
0
-5
-10 Degrees Latitude

Fig. 15

Tropical Cyclone Paka

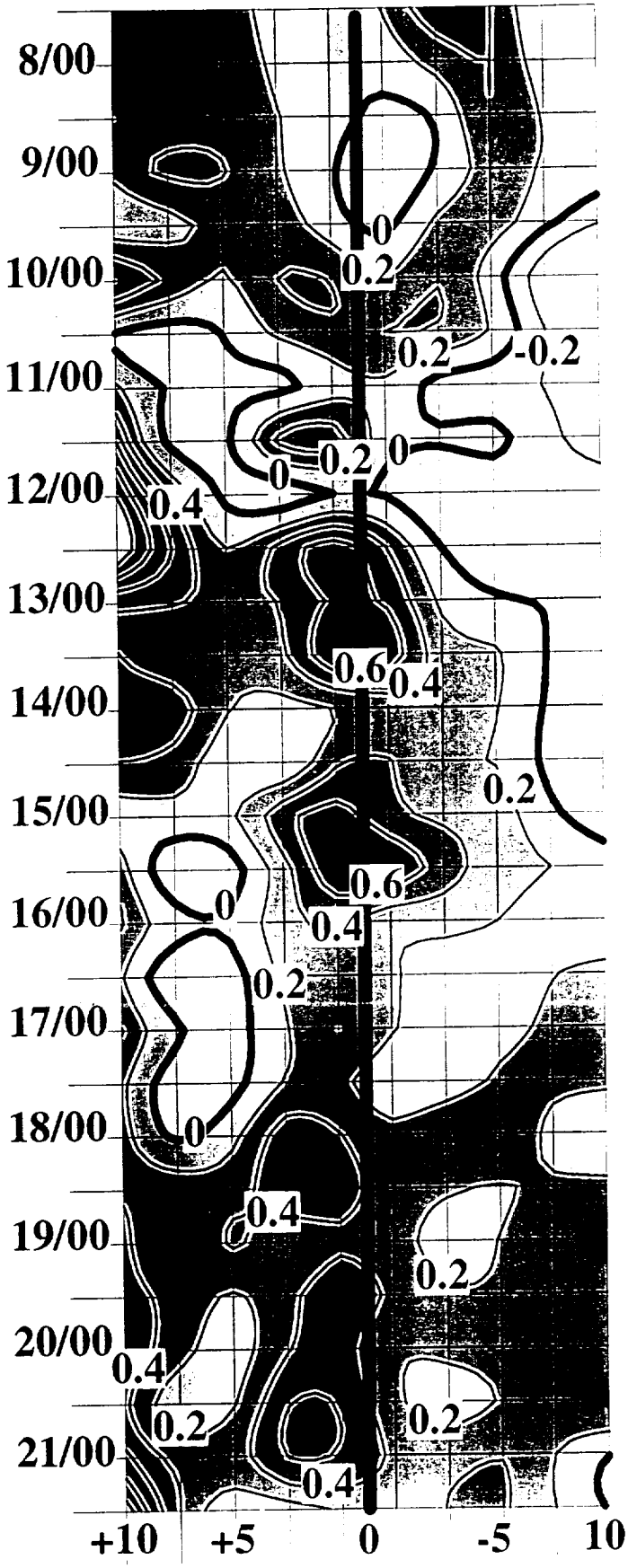

Fig. 16

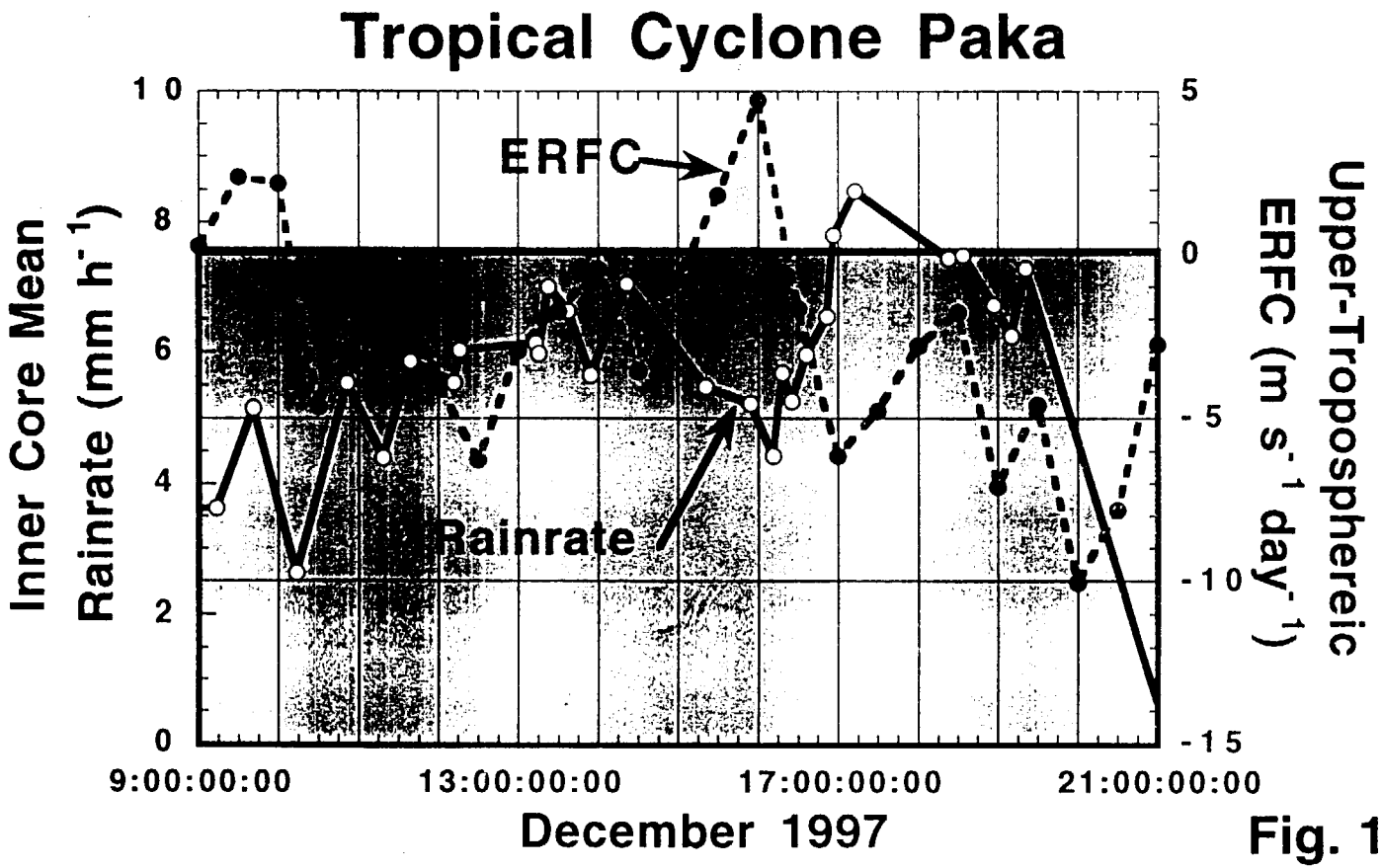
Tropical Cyclone Paka
Inner Core Mean
Rainrate (mm h-1)
Upper-Tropospheric
ERFC (m s-1 day-1)
ERFC
Rainrate
10
8
6
4
2
0
5
0
-5
-10
-15
9:00:00:00
13:00:00:00
17:00:00:00
21:00:00:00
December 1997

Fig. 17

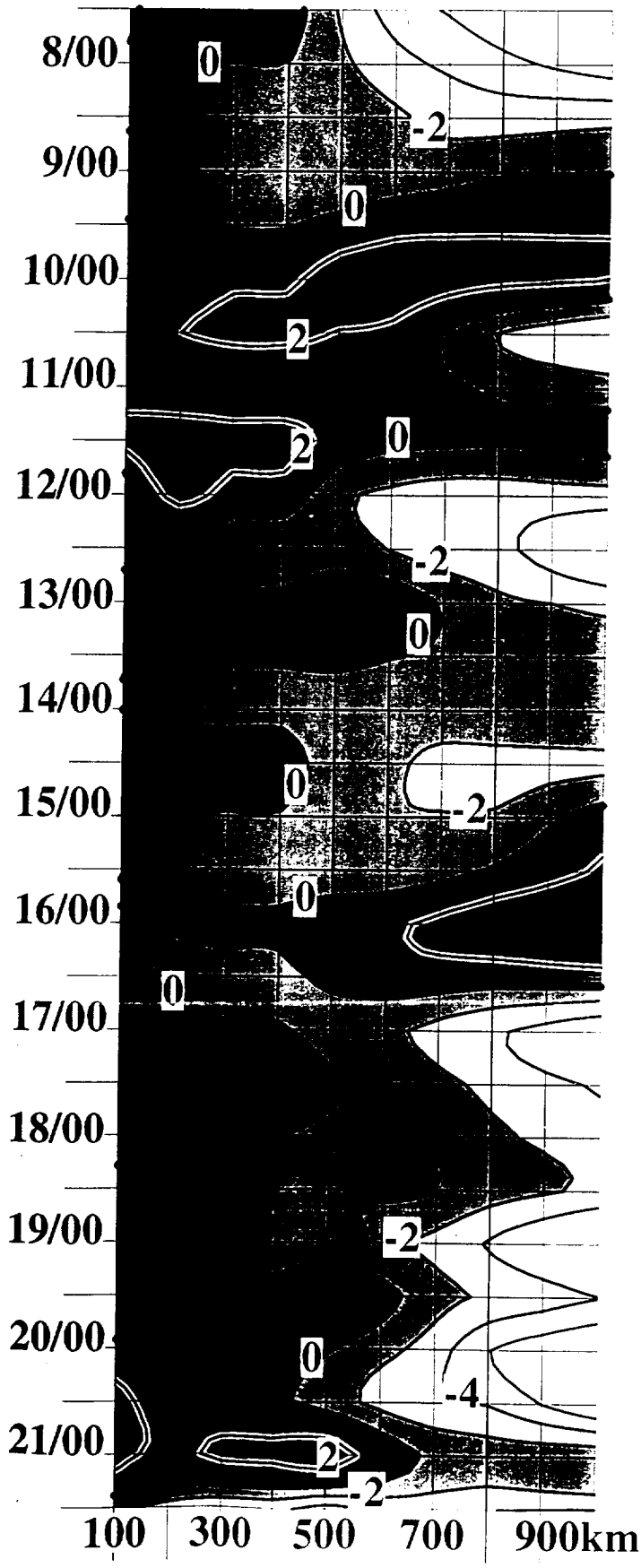
Tropical Cyclone Paka
8/00
9/00
10/00
11/00
12/00
13/00
14/00
15/00
16/00
17/00
18/00
19/00
20/00
21/00
0
-2
0
2
2
0
-2
0
0
-2
0
0
-2
0
-4
2
-2
100
300
500
700
900km

Fig. 18